Electronic Supplementary Material (ESI) for Materials Chemistry Frontiers.

# Molecular Mechanism of Rigidity- and Planarity-Promoted, State-Dependent Doping of Conjugated Ladder-Type Molecules

*Jongbok Lee*,‡,1,3, Shi Li‡,1, Xiaozhou Ji1, Sai Che1, Yirui Cao1, Daniel P. Tabor*1, and*

*Lei Fang*,1,2*

---

*1. Department of Chemistry, Texas A&M University, 3255 TAMU, College Station, TX, USA*

*2. Department of Materials Science & Engineering, Texas A&M University, 3003 TAMU, College Station, TX, USA*

*3. Department of Biological and Chemical Engineering, Hongik University, 2639, Sejong-ro, Jochiwon-eup, Sejong-si, Korea*

---

## *Supporting Information*

***Correspondence Address**

**Dr Jongbok Lee**: Department of Biological and Chemical Engineering, Hongik University, 2639, Sejong-ro, Jochiwon-eup, Sejong-si, 30016, Korea; E-Mail: jlee0917@hongik.ac.kr

**Dr Daniel P. Tabor**: Department of Chemistry, Texas A&M University, 3255 TAMU, College Station, TX 77843-3255, USA; E-Mail: daniel_tabor@tamu.edu

**Dr Lei Fang**: Department of Chemistry, Texas A&M University, 3255 TAMU, College Station, TX 77843-3255, USA; E-Mail: fang@chem.tamu.edu

# Table of Contents

## 1. General information

Starting materials and reagents were purchased from Alfa Aesar, Combi-blocks, Oakwood, and Suna-tech and used as received without further purification. Toluene and THF were dried using a pure solvent system (PureSolv-MD-5) and used without further treatment. Compounds **S4** (3,6-bis(1-methylethenyl)-9-(1-octylnonyl)-2,7-bis(4,4,5,5-tetramethyl-1,3,2-dioxaborolan-2-yl)-9*H*-carbazole),[1] **1** (2,8-diethenyl-3,9-bis(4,4,5,5-tetramethyl-1,3,2-dioxaborolan-2-yl)-5,11-dihydro-5,11-di(1-octylnonyl)indolo[3,2-b]carbazole),[2] **S1** (4-bromo-5-methyl-2,1,3-benzothiadiazole),[3] and **B-Cz**[1] were synthesized according to procedure reported in the literatures. Analytical thin-layer chromatography was performed on glass that is precoated with silica gel 60-F254 (Sorbtech). Flash column chromatography was carried out using Biotage® Isolera™ Prime instrument with various size of $SiO_2$ Biotage ZIP® cartridge. UV/vis absorption spectra were recorded using Shimadzu UV-2600. Fluorescent emission spectra were measured on Horiba Fluoromax-4. UV-vis-NIR spectra were measured on a Hitachi U-4100 spectrometer. FT-IR spectra were recorded with ZnSe ATR using Shimadzu IRAffinity-1S. Cyclic voltammograms were recorded with Bio-Logic Science SP200 potentiostat. $^1H$ and $^{13}C$ NMR spectra were obtained on a 500 MHz Varian Inova at room temperature and processed by MestReNova 9.0. Chemical shifts are reported in ppm relative to the signals corresponding to the residual non-deuterated solvents ($CDCl_3$: $\delta$ 7.26 for $^1H$ and 77.16 for $^{13}C$ at room temperature). Preparative size exclusion chromatography (SEC) was performed in chloroform solution at room temperature using JAI recycling preparative HPLC (LC-92XXII NEXT SERIES). High-resolution Matrix-assisted laser desorption/ionization (HR-MALDI) mass spectra were measured on Applied Biosystems 4800 MALDI-TOF. Electron paramagnetic resonance (EPR) spectroscopy was conducted on a Bruker ELEXSYS II E500 with microwave frequency of *ca.*

9.38 GHz at 288 K. 1 mm ID sample tubes were used for solutions and 4 mm ID sample tubes were used for solids. The spectra were acquired at 1 G modulation and 100 kHz modulation frequency. The microwave power was 0.1 mW for solutions and 0.6 mW for solids. X-ray single crystal diffraction measurement was made on a BRUKER APEX 2 X-ray (three-circle) diffractometer. The X-ray radiation employed was generated from a Mo sealed X-ray tube (K = 0.70173Å with a potential of 40 kV and a current of 40 mA) fitted with a graphite monochromator in the parallel mode (175 mm collimator with 0.5 mm pinholes). Detailed computational methods are described in **section S4**.

## 2. Synthesis

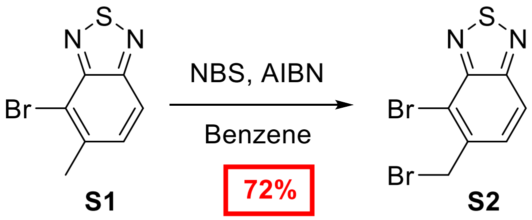

**Scheme S1**. Synthesis of compound **S2** (4-bromo-5-(bromomethyl)-2,1,3-benzothiadiazole) from **S1**.

**S2 (4-bromo-5-(bromomethyl)-2,1,3-benzothiadiazole)**: Compound **S1** (3.6 g, 15.7 mmol) was dissolved in anhydrous benzene (120 mL) under nitrogen atmosphere at room temperature. To the mixture were added *N*-Bromosuccinimide (NBS) (3.1 g, 17.2 mmol) and azobisisobutyronitrile (AIBN) (0.3 g, 0.17 mmol). The mixture was stirred and refluxed for 16 h. After being cooled to room temperature, the precipitate was filtered and washed with hexane. The filtrate was concentrated under reduced pressure and recrystallized using $CHCl_3$/EtOH to give the product **S2** (3.5 g, 72%) as a white solid. $^1$H NMR (500 MHz, $CDCl_3$): δ 7.95 (d, $J = 9.0$

Hz, 1H), 7.68 (d, *J* = 9.0 Hz, 1H), 4.80 (s, 2H). $^{13}$C NMR (125 MHz, CDCl$_3$): δ 154.0, 153.9, 138.6, 132.0, 121.0, 116.0, 30.3. LR-APCI: calcd. For $C_7H_5Br_2N_2S$ [*M*+H]$^+$ m/z = 308.85; found m/z = 308.95.

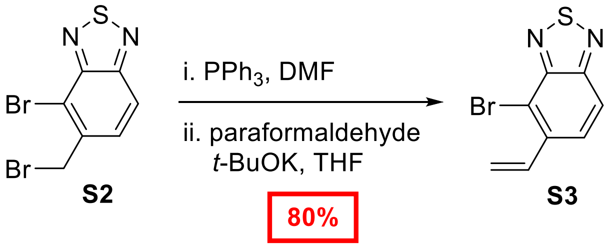

**Scheme S2**. Synthesis of compound **S3** (4-bromo-5-ethenyl-2,1,3-benzothiadiazole) from **S2**.

**S3 (4-bromo-5-ethenyl-2,1,3-benzothiadiazole)**: A mixture of compound **S2** (3.4 g, 9.2 mmol) and PPh$_3$ (6.0 g, 23.0 mmol) in DMF (50 mL) was stirred at 80 °C for 18 h. After being cooled to room temperature, the reaction mixture was concentrated under reduced pressure. The mixture was subsequently added into THF (90 mL) with paraformaldehyde (6.3 g) under N$_2$ to form a suspension. While stirring, *t*-BuOK (3.1 g, 27.6 mmol) was added in small portions over 10 min. After 30 min, the reaction was quenched with water and extracted with CH$_2$Cl$_2$ (3 × 30 mL). The combined organic layer was dried over MgSO$_4$, filtered through Celite, and concentrated under reduced pressure. The residue was purified by flash column chromatography (SiO$_2$, hexane) to give the product **S3** (2.1 g, 80%) as a white solid. $^1$H NMR (500 MHz, CDCl$_3$): δ 7.90 (d, *J* = 9.0 Hz, 1H), 7.84 (d, *J* = 9.0 Hz, 1H), 7.30 (dd, $J_1$ = 17.5 Hz, $J_2$ = 11.0 Hz, 1H), 5.97 (d, *J* = 17.5 Hz, 1H), 5.64 (d, *J* = 11.0 Hz, 1H). $^{13}$C NMR (125 MHz, CDCl$_3$): δ 154.2, 153.8, 137.3, 134.5, 128.0, 120.0, 119.7, 114.2. LR-APCI: calcd. For $C_8H_6BrN_2S$ [*M*+H]$^+$ m/z = 240.94; found m/z = 240.81.

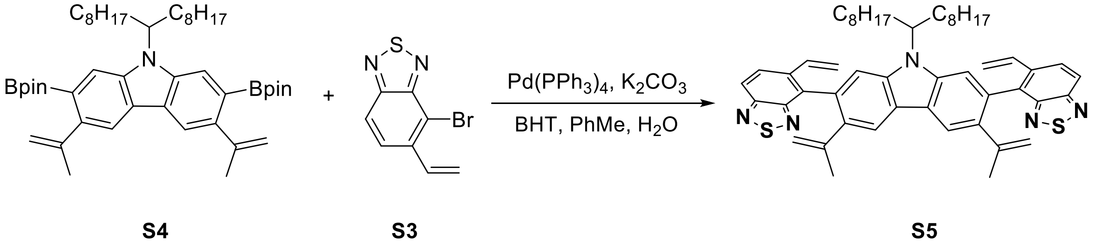

**Scheme S3**. Synthesis of compound **S5** from **S4** and **S3** *via* Suzuki coupling reaction.

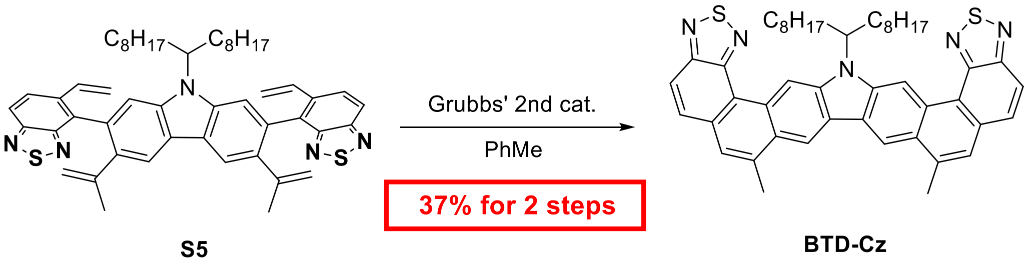

**Scheme S4**. Synthesis of compound **BTD-Cz** from **S5** *via* ring-closing olefin metathesis.

**S5** and **BTD-Cz**: Under nitrogen atmosphere, $Pd(PPh_3)_4$ (31 mg, 10 mol%) was added to a mixture of compound **S4** (200 mg, 0.27 mmol), $K_2CO_3$ (220 mg, 1.62 mmol), aliquat 336 (30 µL, 0.06 mmol), several crystals of 2,6-di-*t*-butyl-4-methylphenol (BHT), and **S3** (200 mg, 0.81 mmol) in degassed toluene (5 mL) and water (0.8 mL). The solution was further degassed by freeze-pump-thaw 3 times, and the reaction mixture covered by aluminum foil was stirred at 100 °C for 24 h. After being cooled to room temperature, the reaction mixture was concentrated under reduced pressure, and the residue was extracted with DCM (3 × 10 mL). The combined organic layer was dried over $MgSO_4$, filtered through Celite, and concentrated under reduced pressure. The residue was purified by flash column chromatography ($SiO_2$, hexane:DCM = 94:6 to 30:70) to give the crude product of **S5**, which was used for the next step without further purification due to the difficulty of purification.

The mixture of crude product of **S5** (150 mg) and Grubbs' 2nd generation catalyst (4 mg, 0.005 mmol) in degassed toluene (7 mL) was stirred at reflux under $N_2$. Immediately, another portion of Grubbs' 2nd generation catalyst (12 mg, 0.014 mmol) in degassed toluene (5 mL) was added slowly for 4 h using syringe pump. Subsequently, the reaction mixture was stirred for an additional 2 h at reflux temperature. After being cooled to room temperature, the reaction mixture was concentrated under reduced pressure, and the residue was filtered through silica pad with 10% $CH_2Cl_2$ in hexane. The product was further purified by preparative SEC to give the product **BTD-Cz** (75 mg, 37% for 2 steps) as a red solid. $^1$H NMR (500 MHz, $CDCl_3$): δ 11.04 (1H)$^\dagger$, 10.86 (1H)$^\dagger$, 9.14 (bs, 2H), 8.05 (dd, $J_1$ = 18.0 Hz, $J_2$ = 9.0 Hz, 4H), 7.70 (s, 2H), 5.27 (m, 1H), 3.12 (s, 6H), 2.95 (m, 2H), 2.31 (m, 2H), 1.25 (m, 24H), 0.62 (t, $J$ = 7.0 Hz, 6H). $^\dagger$Peak separations were observed due to the atropisomers by hindered rotation of α-branched alkyl chain. $^{13}$C NMR (125 MHz, $CDCl_3$): δ 155.4, 154.3, 145.8, 141.8, 137.4, 133.4, 133.0, 130.7, 130.1, 128.5, 126.9, 124.2, 121.1, 119.9, 116.4, 108.6, 106.2, 56.7, 33.2, 31.8, 29.9, 29.51, 29.46, 29.3, 26.9, 22.6, 21.0, 14.0. ($^{13}$C NMR showed multiple separated peaks due to the atropisomers). HR-MALDI: calcd. for $C_{47}H_{52}N_5S_2$ $[M\text{+H}]^+$ m/z = 750.3664; found m/z = 750.3671. Single crystal X-ray diffraction data are described in **Section S4**.

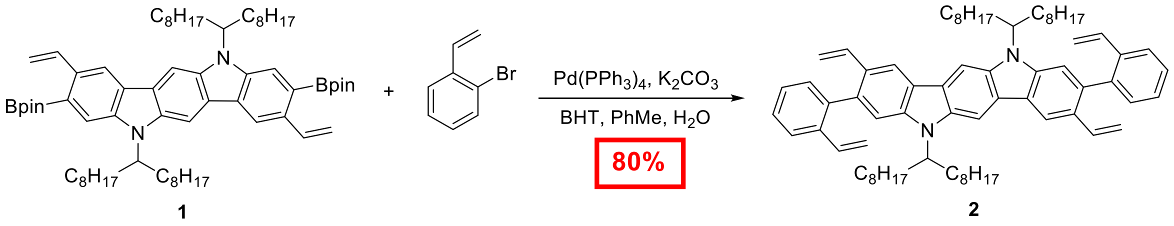

**Scheme S5**. Synthesis of compound **2** from **1** and 2-bromostyrene *via* Suzuki coupling reaction.

**2**: Under nitrogen atmosphere, $Pd(PPh_3)_4$ (16 mg, 10 mol%) was added to a mixture of compound **1** (150 mg, 0.14 mmol), $K_2CO_3$ (110 mg, 0.84 mmol), aliquat 336 (20 μL, 0.04 mmol), several crystals of 2,6-di-*t*-butyl-4-methylphenol (BHT), and 2-bromostyrene (40 μL, 0.42 mmol) in degassed toluene (4 mL) and water (0.8 mL). The solution was further degassed by freeze-pump-thaw 3 times, and the reaction mixture covered by aluminum foil was stirred at 100 °C for 24 h. After being cooled to room temperature, the reaction mixture was concentrated under reduced pressure, and the residue was extracted with DCM (3 × 10 mL). The combined organic layer was dried over $MgSO_4$, filtered through Celite, and concentrated under reduced pressure. The residue was purified by flash column chromatography ($SiO_2$, hexane). The product was further purified by preparative SEC to give the product **2** (0.11 g, 80%) as a yellow solid. $^1$H NMR (500MHz, $CDCl_3$): δ $^†$8.50 (2H), $^†$8.22 (1H), $^†$8.08 (1H), 7.72 (d, *J* = 8.0 H, 2H), 7.42 (m, 2H), 7.34 (m, 5H), 7.18 (s, 1H), 6.53 (m, 4H), 5.78 (dd, $J_1$ = 17.5 Hz, $J_2$ = 8.5 Hz, 2H), 5.68 (d, *J* = 17.5 Hz, 2H), 5.07 (d, *J* = 11.0 Hz, 4H), $^†$4.64 (2H), 2.50 (m, 2H), 2.27 (m, 2H), 1.95 (m, 4H), 1.13 (m, 48H), 0.79 (t, *J* = 7.0 Hz, 12H). $^†$Peak separation was observed due to the atropisomers by hindered rotation of α-branched alkyl chain and vinyl groups. $^{13}$C NMR (125 MHz, $CDCl_3$): δ 151.7, 142.8, 141.1, 141.0, 139.3, 138.1, 127.4, 136.9, 136.8, 136.2, 135.9, 135.7, 135.6, 134.5, 131.2, 131.0, 128.4, 127.6, 127.3, 127.1, 127.0, 125.7, 125.1, 124.9, 122.3, 116.8, 116.4, 116.1, 114.5, 112.9, 111.6, 110.3, 102.0, 99.3, 56.8, 34.4, 33.8, 31.9, 31.6, 31.2, 30.8, 30.5, 30.1, 29.6, 29.4, 27.0, 22.7, 21.3, 14.2. ($^{13}$C NMR showed multiple separated peaks due to the atropisomers). HR-MALDI: calcd for $C_{72}H_{97}N_2$ $[M+H]^+$ $m/z$ = 989.7652; found $m/z$ = 989.7648.

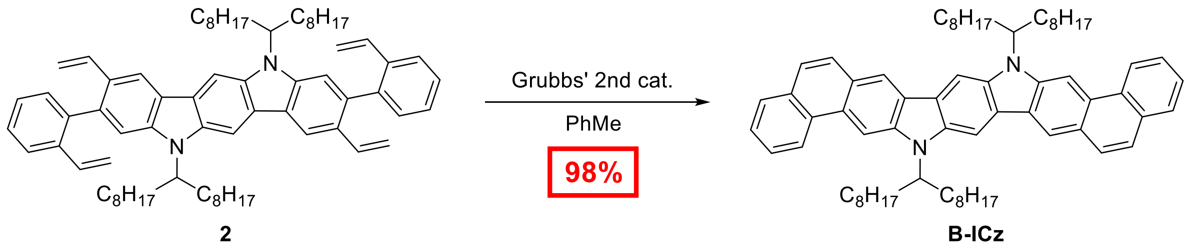

**Scheme S6**. Synthesis of compound **B-ICz** from **5** *via* ring-closing olefin metathesis.

**B-ICz**: The mixture of compound **2** (60 mg, 0.061 mmol) and Grubbs' 2$^{nd}$ generation catalyst (2 mg, 4 mol%) in degassed toluene (5 mL) was stirred at reflux under $N_2$. Immediately, another portion of Grubbs' 2$^{nd}$ generation catalyst (3 mg, 6 mol%) in degassed toluene (3 mL) was added for 4 h using syringe pump. After that, the reaction mixture was stirred for an additional 2 h at reflux temperature. After being cooled to room temperature, the reaction mixture was concentrated under reduced pressure, and the residue was filtered through silica pad with 10% $CH_2Cl_2$ in hexane to give the product **B-ICz** (56 mg, 98%) as a yellow solid. $^1$H NMR (500MHz, $CDCl_3$): δ $^{\dagger}$8.86 (1H), $^{\dagger}$8.81 (2H), $^{\dagger}$8.74 (2H), 8.63 (s, 1H), $^{\dagger}$8.40 (1H), $^{\dagger}$8.25 (1H), $^{\dagger}$7.98 (2H), $^{\dagger}$7.93 (2H), $^{\dagger}$7.72 (2H), 7.64 (m, 4H), $^{\dagger}$4.93 (2H), 2.61 (m, 4H), 2.16 (m, 4H), 1.13 (m, 48H), 0.79 (t, $J$ = 7.0 Hz, 12H). $^{\dagger}$Peak separation was observed due to the atropisomers by hindered rotation of α-branched alkyl chain. $^{13}$C NMR (125 MHz, $CDCl_3$): δ 143.5, 140.0, 135.5, 132.4, 130.6, 129.6, 128.7, 128.0, 126.4, 126.1, 125.3, 124.3, 123.6, 123.5, 122.8, 119.5, 119.3, 102.7, 100.0, 56.8, 33.9, 31.9, 29.9, 29.7, 29.5, 29.3, 27.2, 22.7, 14.1. ($^{13}$C NMR showed multiple separated peaks due to the atropisomers). HR-MALDI: calcd for $C_{68}H_{89}N_2$ $[M+H]^+$ $m/z$ = 933.7026; found $m/z$ = 933.7027. Single crystal X-ray diffraction data are described in **Section S4.**

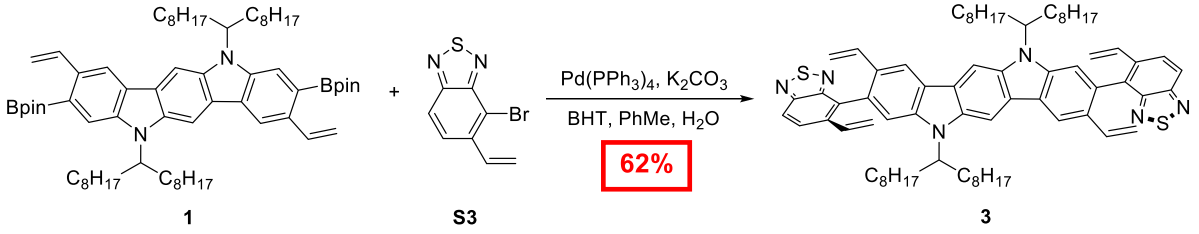

**Scheme S7**. Synthesis of compound **3** from **1** and **S3** *via* Suzuki coupling reaction.

**3**: Under nitrogen atmosphere, $Pd(PPh_3)_4$ (12 mg, 10 mol%) was added to a mixture of compound **1** (100 mg, 0.096 mmol), $K_2CO_3$ (80 mg, 0.58 mmol), aliquat 336 (10 µL, 0.02 mmol), several crystals of 2,6-di-*t*-butyl-4-methylphenol (BHT), and **S3** (70 mg, 0.29 mmol) in degassed toluene (3 mL) and water (0.6 mL). The solution was further degassed by freeze-pump-thaw 3 times, and the reaction mixture covered by aluminum foil was stirred at 100 °C for 24 h. After being cooled to room temperature, the reaction mixture was concentrated under reduced pressure, and the residue was extracted with DCM (3 × 10 mL). The combined organic layer was dried over $MgSO_4$, filtered through Celite, and concentrated under reduced pressure. The residue was purified by flash column chromatography ($SiO_2$, hexane:$CH_2Cl_2$ = 88:12 to 0:100). The product was further purified by preparative SEC to give the product **3** (66 mg, 62%) as a brown solid. $^1H$ NMR (500MHz, $CDCl_3$): δ $^{\dagger}$8.61 (2H), $^{\dagger}$8.27 (1H), $^{\dagger}$8.13 (1H), 8.05 (s, 4H), $^{\dagger}$7.41 (1H), $^{\dagger}$7.25 (1H), 6.72 (m, 2H), 6.41 (dd, $J_1$ = 17.5 Hz, $J_2$ = 11.0 Hz, 2H), 5.92 (d, $J$ = 17.5 Hz, 2H), 5.82 (d, $J$ = 17.5 Hz, 2H), 5.32 (d, $J$ = 11.0 Hz, 2H), 4.99 (d, $J$ = 11.0 Hz, 2H), $^{\dagger}$4.65 (2H), 2.51 (m, 2H), 2.26 (m, 2H), 1.96 (m, 4H), 1.13 (m, 48H), 0.80 (t, $J$ = 7.0 Hz, 12H). $^{\dagger}$Peak separations were observed due to the atropisomers by hindered rotation of α-branched alkyl chain. $^{13}C$ NMR (125 MHz, $CDCl_3$): δ 156.1, 154.5, 151.7, 143.0, 139.5, 138.7, 136.2, 136.0, 135.6, 134.4, 133.0, 132.6, 132.1, 128.4, 127.5, 125.7, 124.7, 123.3, 120.5, 117.1, 116.9, 116.7, 113.4, 112.2, 110.7, 102.1, 99.4, 56.8, 34.1, 33.9, 33.7, 31.9, 30.5, 29.9, 29.7, 29.5, 29.4, 27.1, 27.0, 22.7, 14.2. ($^{13}C$

NMR showed multiple separated peaks due to the atropisomers). HR-MALDI: calcd for $C_{72}H_{93}N_6S_2$ $[M\text{+H}]^+$ $m/z = 1105.6903$; found $m/z = 1105.6900$.

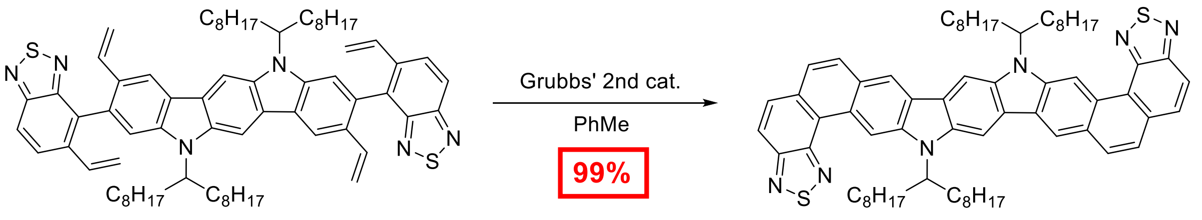

**3**

**BTD-ICz**

**Scheme S8**. Synthesis of compound **BTD-ICz** from **3** *via* ring-closing olefin metathesis.

**BTD-ICz**: The mixture of compound **3** (50 mg, 0.04 mmol) and Grubbs' 2nd generation catalyst (2 mg, 5 mol%) in degassed toluene (5 mL) was stirred at reflux under $N_2$. Immediately, another portion of Grubbs' 2nd generation catalyst (3 mg, 8 mol%) in degassed toluene (3 mL) was added for 4 h using syringe pump. After that, the reaction mixture was stirred for an additional 2 h at reflux temperature. After being cooled to room temperature, the reaction mixture was concentrated under reduced pressure, and the residue was filtered through silica pad with 10% $CH_2Cl_2$ in hexane to give the product **BTD-ICz** (48 mg, 99%) as a red solid. $^1$H NMR (500 MHz, $CDCl_3$): δ $^{\dagger}$10.93 (1H), $^{\dagger}$10.75 (1H), $^{\dagger}$8.92 (2H), $^{\dagger}$8.51 (1H), $^{\dagger}$8.37 (3H), 8.09 (dd, $J_1 = 15.5$ Hz, $J_2 = 9.0$ Hz, 4H), $^{\dagger}$7.83 (2H), $^{\dagger}$5.10 (2H), 2.85 (m, 2H), 2.69 (m, 2H), 2.25 (m, 4H), 1.05 (m, 48H), 0.68 (t, $J = 7.0$ Hz, 12H). $^{\dagger}$Peak separations were observed due to the atropisomers by hindered rotation of α-branched alkyl chain. $^{13}$C NMR (125 MHz, $CDCl_3$): δ 155.5, 154.5, 145.3, 141.3, 139.8, 136.0, 135.9, 133.6, 132.9, 131.3, 129.6, 129.0, 127.0, 126.9, 125.8, 124.8, 123.0, 122.1, 119.6, 119.4, 107.8, 105.4, 102.8, 100.1, 57.2, 56.6, 33.8, 33.3, 31.8, 29.9, 29.7, 29.5, 29.4, 29.3, 27.1, 22.6, 14.1. ($^{13}$C NMR showed multiple separated peaks due to the atropisomers). HR-

MALDI: calcd for $C_{68}H_{85}N_6S_2$ $[M+H]^+$ $m/z$ = 1049.6277; found $m/z$ = 1049.6285. Single crystal X-ray diffraction data are described in **Section S4**.

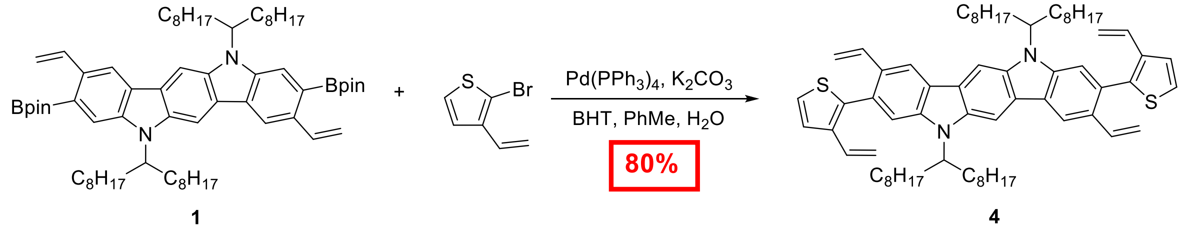

**Scheme S9**. Synthesis of compound **4** from **1** and 2-bromo-3-vinylthiophene *via* Suzuki coupling reaction.

**4**: Under nitrogen atmosphere, $Pd(PPh_3)_4$ (0.11 g, 0.09 mmol) was added to a mixture of compound **1** (0.92 g, 0.88 mmol), $K_2CO_3$ (0.73 g, 5.32 mmol), aliquat 336 (100 mg, 0.22 mmol), several crystals of BHT, and 2-bromo-3-vinylthiophene (0.5 g, 2.66 mmol) in degassed toluene (20 mL) and water (4 mL). The solution was further degassed by freeze-pump-thaw 3 times, and the reaction mixture covered by aluminum foil was stirred at 100 °C for 24 h. After being cooled to room temperature, the reaction was quenched with water and diluted with $CH_2Cl_2$. The mixture was extracted with $CH_2Cl_2$ (3 × 30 mL) and the combined organic layer was dried over $MgSO_4$, filtered through Celite, and concentrated under reduced pressure. The residue was purified by flash column chromatography ($SiO_2$, hexane/$CH_2Cl_2$ 98:2). The product was further purified by preparative SEC to give product **4** (0.70g, 80%) as a yellow solid. $^1H$ NMR (500 MHz, $CDCl_3$): δ $^\dagger$8.49 (2H), $^\dagger$8.21 (1H), $^\dagger$8.14 (1H), $^\dagger$7.48 (1H), 7.37 (m, 4H), $^\dagger$7.32 (1H), 6.81 (m, 2H), 6.43 (m, 2H), 5.83 (dd, $J_1$ = 17.5 Hz, $J_2$ = 9.0 Hz, 2H), 5.57 (d, $J$ = 15.5 Hz, 2H), 5.14 (d, $J$ = 11.0 Hz, 2H), 5.12 (d, $J$ = 11.0 Hz, 2H), $^\dagger$4.65 (2H), 2.49 (m, 2H), 2.29 (m, 2H), 2.00 (m, 4H), 1.09 (m, 48H), 0.79 (t, $J$ = 7.0 Hz, 12H). $^\dagger$Peak separations were observed due to the atropisomers by hindered rotation of α-branched alkyl chain. $^{13}C$ NMR (125 MHz, $CDCl_3$): δ

142.7, 140.0, 139.2, 138.7, 137.5, 136.1, 134.8, 130.6, 130.2, 129.6, 128.4, 125.0, 124.6, 124.2, 123.9, 123.3, 122.8, 122.5, 116.9, 116.6, 114.2, 113.7, 112.2, 111.7, 102.1, 99.3, 56.8, 33.9, 33.8, 31.9, 29.7, 29.5, 29.4, 29.3, 27.0, 22.7, 14.2. ($^{13}$C NMR showed multiple separated peaks due to the atropisomers). HR-MALDI: calcd for $C_{68}H_{93}N_2S_2$ $[M+H]^+$ $m/z$ = 1001.6780; found $m/z$ = 1001.6778.

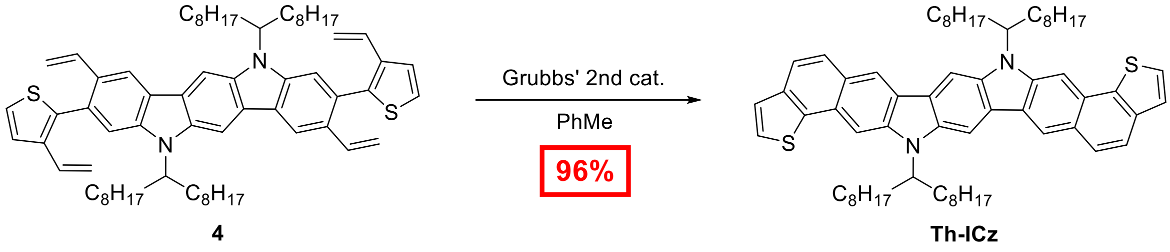

**Scheme S10**. Synthesis of compound **Th-ICz** from **7** *via* ring-closing olefin metathesis.

**Th-ICz**: The mixture of compound **4** (0.27 g, 0.27 mmol) and Grubbs' 2nd generation catalyst (8 mg, 0.009 mmol) in degassed toluene (30 mL) was stirred at reflux under $N_2$. Immediately, another portion of Grubbs' 2nd generation catalyst (15 mg, 0.018 mmol) in degassed toluene (3 mL) was added for 4 h using syringe pump. After that, the reaction mixture was stirred for an additional 2 h at reflux temperature. The mixture was diluted with $CH_2Cl_2$ and concentrated under reduced pressure. The residue was purified by flash column chromatography ($SiO_2$, hexane). The product was further purified by preparative SEC to give product **Th-ICz** (0.25 g, 96%) as a yellow solid. $^1$H NMR (500 MHz, $CDCl_3$): δ $^†$8.77 (2H), $^†$8.33 (1H), $^†$8.17 (2H), $^†$7.97 (3H), 7.75 (d, $J$ = 11.0 Hz, 2H), 7.52 (dd, $J_1$ = 11.0 Hz, $J_2$ = 5.5 Hz, 4H), 4.84 (bs, 2H), 2.56 (m, 4H), 2.12 (m, 4H), 1.13 (m, 48H), 0.74 (t, $J$ = 7.0 Hz, 12H). $^†$Peak separations were observed due to the atropisomers by hindered rotation of α-branched alkyl chain. $^{13}$C NMR (125 MHz,

$CDCl_3$): δ 143.6, 139.8, 139.5, 137.0, 136.8, 135.6, 128.4, 128.0, 126.1, 125.7, 124.5, 124.4, 124.2, 123.1, 122.8, 119.8, 119.6, 118.8, 118.7, 102.4, 99.6, 57.0, 33.8, 33.5, 31.9, 29.7, 29.5, 29.3, 27.1, 22.7, 14.1. ($^{13}C$ NMR showed multiple separated peaks due to the atropisomers). HR-MALDI: calcd for $C_{64}H_{85}N_2S_2$ $[M+H]^+$ $m/z$ = 945.6154; found $m/z$ = 945.6155. Single crystal X-ray diffraction data are described in **Section S4.**

## 3. Computational Methods

***Complex geometry sampling***. We obtained complex geometries for further electronic structure analysis in a two-step procedure. First, the conformations of the ladder-type molecules and corresponding precursor molecules were sampled with CREST program;[4] geometries were optimized using the semi-empirical GFN2-xTB method.[5-7] The octyl chains were retained in the initial sampling, due to potential steric effects that could affect the potentially realizable geometries for complexes of $F_4TCNQ$ with the other molecules. For each molecule, the conformers within 5 kcal/mol energy of the minimum (at GFN2-xTB) were selected and mixed with the $F_4TCNQ$ to build 1000 random complex structures. The geometry of the complex was optimized at the same GFN2-xTB level of theory,[8] with the ORCA 4.2.1 package.[9]

For each donor molecule, we analyzed the charge-transfer character five complexes with the lowest energies were selected for charge transfer analysis.

***Charge transfer calculations:*** To determine the extent that charge transfer (and other non-covalent interactions) affect the molecular complex geometry and energetics, we employed second-generation absolutely localized molecular orbital energy decomposition analysis (ALMO-EDA)[10] calculations as implemented in the Q-Chem 5.3 package[11] (ωB97X-D/6-

31+G(d) level of theory).[12] Our specific focus is on the charge-transfer contributions to the interactions and the geometric orientations that promote a high degree of charge-transfer character. Motivated by this, we constructed a “charge-transfer-contribution-only” potential energy surface of the complex structures. We performed a geometry scan between the **ICz** molecules and $F_4TCNQ$, with the GFN2-xTB-optimized-complex structure used as the initial geometry. The backbone of the **ICz** molecule was transformed to the *xy* plane and then the $F_4TCNQ$ was shifted along the *x* and *y* axes at 1 Å interval. At each geometry, the charge transfer characteristics of the complexes were analyzed with ALMO-EDA method. We also shifted the $F_4TCNQ$ along the z direction using the geometries with the highest charge transfer properties found from the charge transfer scan to investigate the change of energy composition as a function of the intermolecular distance. Here, all alkyl chains were replaced with methyl groups, for computational cost considerations and to obtain a full mapping of the potential π-π interactions without their steric effects interfering. The effect of this replacement on the amount of charge transfer was evaluated in **Figure S1**. The charge transfer is decreased by a maximum of 8% for **B-ICz**/$F_4TCNQ$ complex, since the decrease is consistent for each complex, we expect this replacement does not affect the overall charge transfer map.

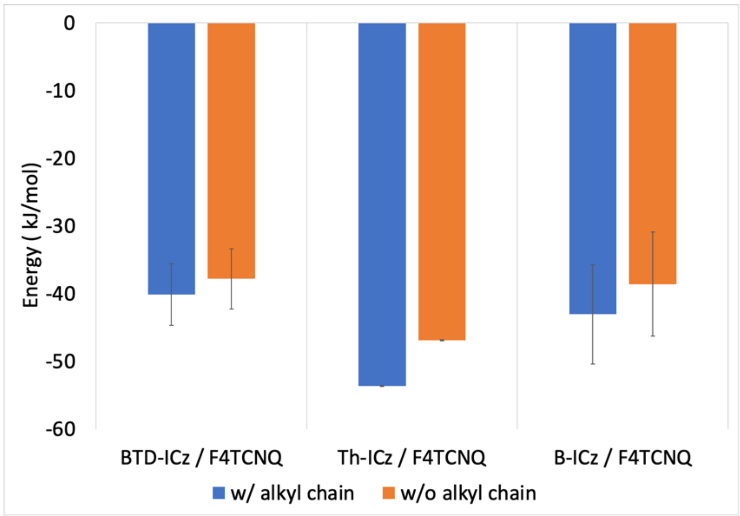

**Figure S1**. Effect of the alkyl chain on the amount of charge transfer of the three **ICz**/$F_4$TCNQ complex calculated at ωB97X-D/6-31+G(d) level of theory.

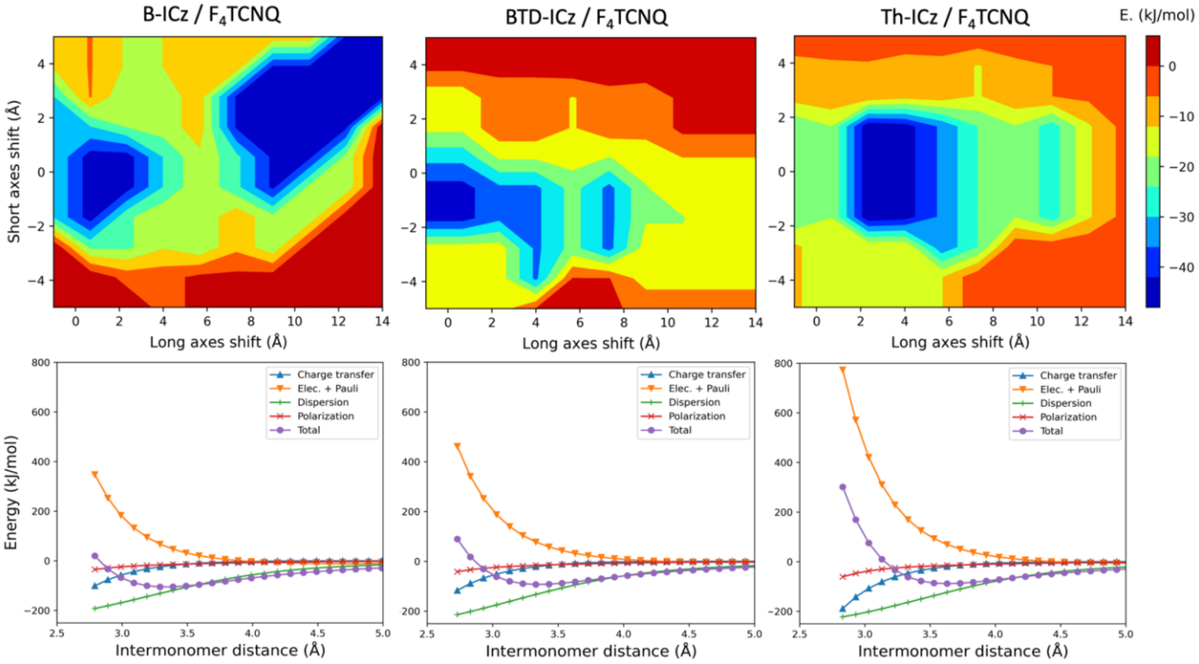

**Figure S2**. (Top) Charge transfer surface of three **ICz**/$F_4$TCNQ complexes calculated by shifting the $F_4$TCNQ along the long and short axes of **ICz** molecules and (Bottom) EDA as a function of intermolecular distance carried out at ωB97X-D/6-31+G(d) level of theory.

As shown in **Figure S2**, the charge transfer region is covered along all **ICz** surfaces, with the largest amount around -50 kJ/mol. Particularly, the high charge transfer region in **BTD-ICz**/$F_4$TCNQ complex is located at the center of the **BTD-ICz** and extends to the end of the molecule, there is a secondary high charge transfer region located about 7 Å away from the center. For the **Th-ICz**/$F_4$TCNQ complex, the highest charge transfer region is located between 3-4 Å away from the center. The **B-ICz**/$F_4$TCNQ also presents two high charge transfer regions, one at 1 Å away from the center of **B-ICz** molecule and the other expands from 9-14 Å.

We changed the $F_4$TCNQ···**ICz** distance in the complex and analyzed the energy decomposition found with the ALMO-EDA method (**Figure S2**). As expected, the charge transfer, polarization, and dispersion energies decrease as the distance between the complexes increases, the dispersion term decreases more rapidly with distance, and the polarization energy is the least sensitive to the stacking distance. While the molecules are separated by more than 4 Å, there is almost no charge transfer energy for all complexes. Instead, the total energy main contribution is from the dispersion term with a small portion contributed by polarization.

## 4. X-ray Crystallography

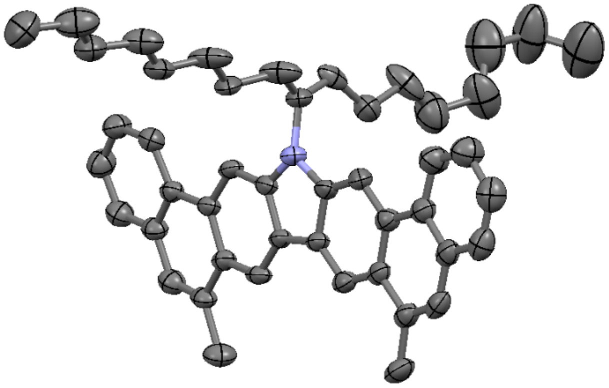

**Figure S3**. Single-crystal X-ray structure of **B-Cz** with probability ellipsoids set at 50% level. Hydrogen atoms have been omitted for clarity.

**B-Cz**: **CCDC-1040797** contains the supplementary crystallographic data for this paper. These data can be obtained free of charge from The Cambridge Crystallographic Data Centre via www.ccdc.cam.ac.uk/data_request/cif. A yellow plate crystal of **B-Cz** having approximate dimensions of 0.435 mm x 0.195 mm x 0.056 mm was mounted on a nylon loop. Cell constants and an orientation matrix for data collection corresponded to a Triclinic cell with dimensions:

| | |
|---|---|
| a = 14.501(4) Å | α = 62.892(4)° |
| b = 20.180(6) Å | β = 84.149(4)° |
| c = 22.027(7) Å | γ = 77.270(4)° |

$V$ = 5597(3) Å$^3$

For Z = 6 and F.W. = 633.92, the calculated density is 1.129 mg/m$^3$. Systematic reflection conditions and statistical tests of the data suggested the space group *P-1*. The data were collected at a temperature of 110.15 K with a theta range for the data collection of 1.039 to 20.870°.

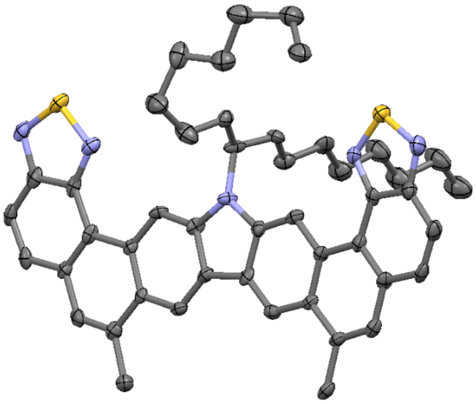

**Figure S4**. Single-crystal X-ray structure of **BTD-Cz** with probability ellipsoids set at 50% level. Hydrogen atoms have been omitted for clarity.

**BTD-Cz**: **CCDC-1840335** contains the supplementary crystallographic data for this paper. These data can be obtained free of charge from The Cambridge Crystallographic Data Centre via www.ccdc.cam.ac.uk/data_request/cif. A red block crystal of **BTD-Cz** having approximate dimensions of 0.388 mm x 0.077 mm x 0.038 mm was mounted on a nylon loop. Cell constants and an orientation matrix for data collection corresponded to a Triclinic cell with dimensions:

| | |
|---|---|
| a = 8.7337(2) Å | α = 106.335(2)° |
| b = 14.0615(4) Å | β = 90.631(2)° |
| c = 17.5080(5) Å | γ = 92.772(2)° |

*V* = 2060.25(10) Å$^3$

For Z = 2 and F.W. = 750.04, the calculated density is 1.209 mg/m$^3$. Systematic reflection conditions and statistical tests of the data suggested the space group *P-1*. The data were collected at a temperature of 100 K with a theta range for the data collection of 2.631 to 62.495°.

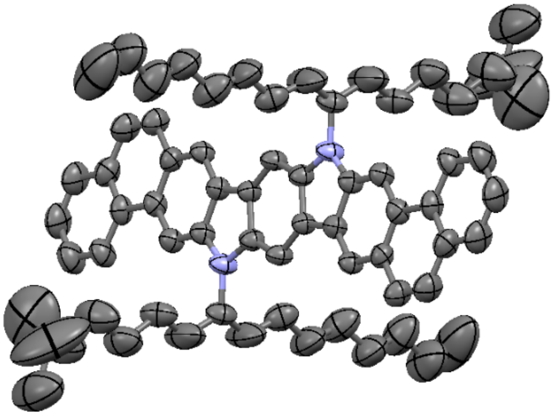

**Figure S5**. Single-crystal X-ray structure of **B-ICz** with probability ellipsoids set at 50% level. Hydrogen atoms have been omitted for clarity.

**B-ICz**: **CCDC-1840336** contains the supplementary crystallographic data for this paper. These data can be obtained free of charge from The Cambridge Crystallographic Data Centre via www.ccdc.cam.ac.uk/data_request/cif. A yellow plate of **B-ICz** having approximate dimensions of 0.15 mm x 0.08mm x 0.06 mm was mounted on a nylon loop. Cell constants and an orientation matrix for data collection corresponded to a Triclinic cell with dimensions:

| | |
|---|---|
| a = 12.531(2) Å | α = 63.164(9)° |
| b = 15.989(2) Å | β = 86.767(16)° |
| c = 16.278(4) Å | γ = 79.355(11)° |

*V* = 2858.8(9) Å$^3$

For Z = 2 and F.W. = 933.40, the calculated density is 1.084 mg/m$^3$. Systematic reflection conditions and statistical tests of the data suggested the space group *P-1*. The data were collected at a temperature of 110 K with a theta range for the data collection of 3.044 to 62.110°.

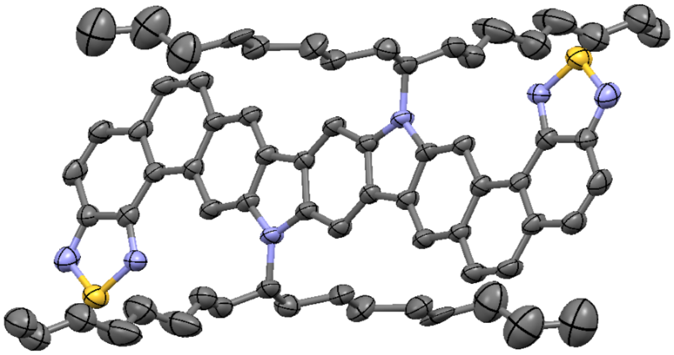

**Figure S6**. Single-crystal X-ray structure of **BTD-ICz** with probability ellipsoids set at 50% level. Hydrogen atoms have been omitted for clarity.

**BTD-ICz**: **CCDC-1840338** contains the supplementary crystallographic data for this paper. These data can be obtained free of charge from The Cambridge Crystallographic Data Centre via www.ccdc.cam.ac.uk/data_request/cif. A red block crystal of **BTD-ICz** having approximate dimensions of 0.07 mm x 0.04 mm x 0.02 mm was mounted on a nylon loop. Cell constants and an orientation matrix for data collection corresponded to a Triclinic cell with dimensions:

| | |
|---|---|
| a = 14.6049(10) Å | α = 80.531(5)° |
| b = 14.8027(10) Å | β = 68.917(4)° |
| c = 15.7342(10) Å | γ = 77.225(5)° |

*V* = 3081.8(4) Å$^3$

For Z = 2 and F.W. = 1088.58, the calculated density is 1.173 mg/m$^3$. Systematic reflection conditions and statistical tests of the data suggested the space group *P-1*. The data were collected at a temperature of 110.15 K with a theta range for the data collection of 3.023 to 60.931°.

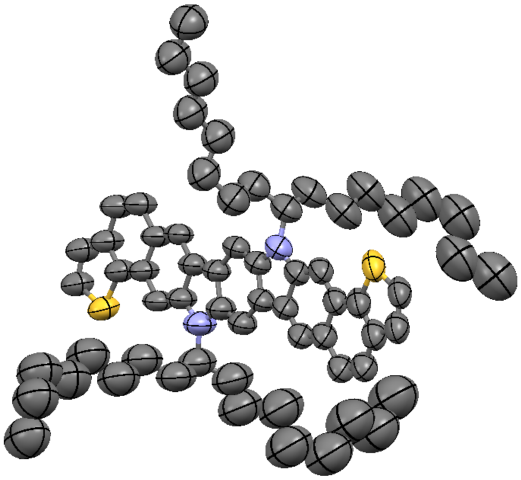

**Figure S7**. Single-crystal X-ray structure of **Th-ICz** with probability ellipsoids set at 50% level. Hydrogen atoms have been omitted for clarity.

**Th-ICz**: **CCDC-1840339** contains the supplementary crystallographic data for this paper. These data can be obtained free of charge from The Cambridge Crystallographic Data Centre via www.ccdc.cam.ac.uk/data_request/cif. A brown block crystal of **Th-ICz** having approximate dimensions of 0.247 mm x 0.139 mm x 0.105 mm was mounted on a nylon loop. Cell constants and an orientation matrix for data collection corresponded to a Triclinic cell with dimensions:

| | |
|---|---|
| a = 22.293(5) Å | α = 90° |
| b = 22.293(5) Å | β = 90° |
| c = 47.638(12) Å | γ = 90° |

*V* = 23674(13) Å$^3$

For Z = 16 and F.W. = 945.45, the calculated density is 1.061 mg/m$^3$. Systematic reflection conditions and statistical tests of the data suggested the space group *I41/a*. The data were collected at a temperature of 110 K with a theta range for the data collection of 1.008 to 16.735°.

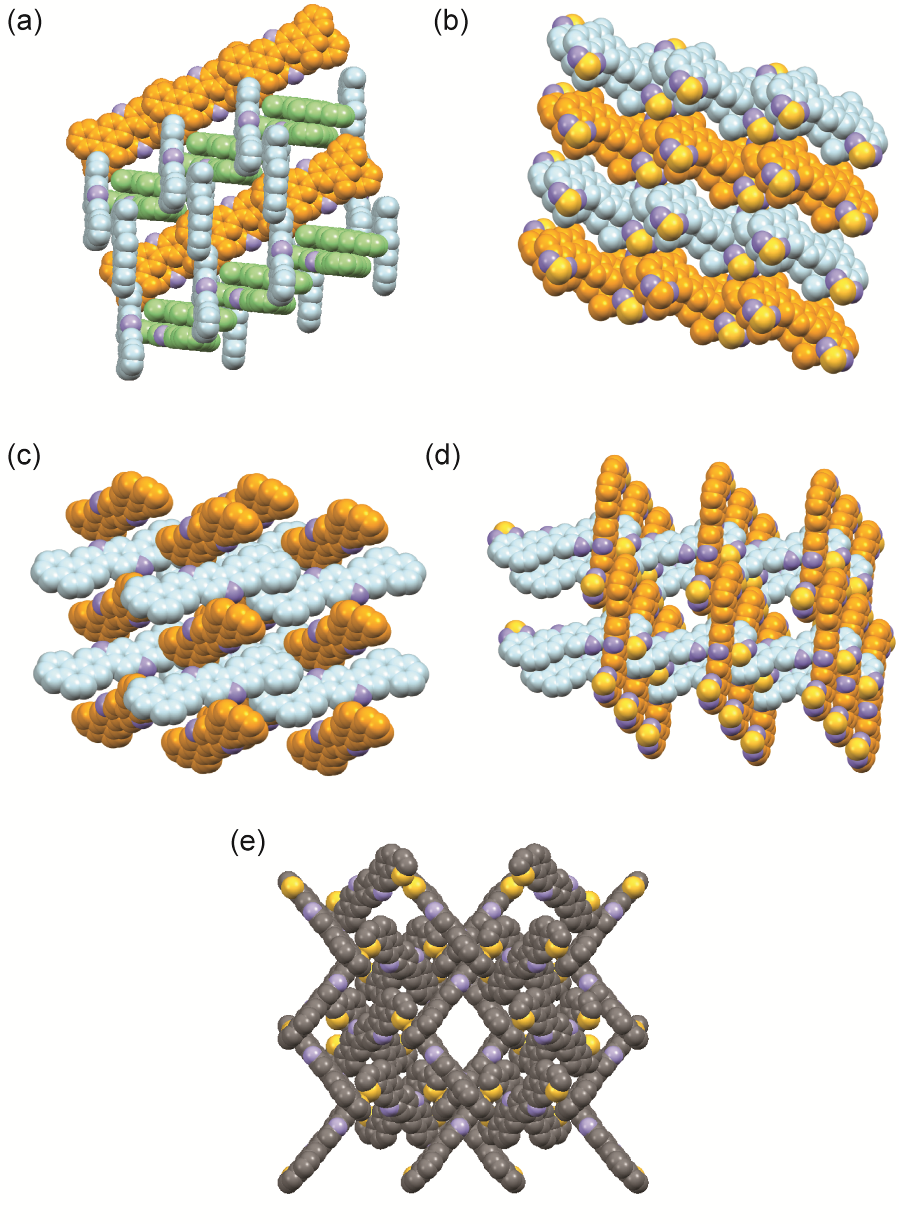

**Figure S8**. Single crystal packing structures of (a) **B-Cz**, (b) **BTD-Cz**, (c) **B-ICz**, (d) **BTD-ICz**, and (e) **Th-ICz**. Alkyl side chains and hydrogen atoms have been omitted for clarity.

The structures of the fused polycyclic heteroarenes were unambiguously confirmed by single crystal X-ray diffraction (**Figure S8**). The crystal structures demonstrated that α-branched alkyl side-chains were perpendicular to the extended backbones interrupting a potential strong intermolecular π-π interaction. Furthermore, all the backbones adopted a rigid coplanar geometry. The crystal structure of **B-Cz** demonstrated that one molecule paired with another molecule upside down in a face-centered stacking manner (green and orange) due to $C_{2v}$ symmetry of the carbazole backbone and the steric hindrance of the alkyl side-chains (**Figure S8a**). The π-π stacking distance of these paired molecules was measured to be 3.40 Å. These paired molecules also exhibited π-π interactions between very small π-faces of the end benzene rings in an off-centered parallel stacking manner with a distance of 3.49 Å. Moreover, the paired molecules were sandwiched by two different sets of paired molecules (orange) orthogonally. In addition, these paired molecules were surrounded by single molecules (blue). **B-Cz** exhibited two different torsional angles based on the stacking manner. The torsional angles of the molecules in a face-stacking (green and orange) were measured to be 0.39° and 0.88°. However, that of peripheral single molecules (blue) were measured to be 1.58° and 4.66°. This result suggests the coplanarization of the rigid backbone induced by stronger π-π interactions. The crystal structure of **BTD-Cz** also exhibited two molecules paired with each other in a face-centered stacking manner (blue and orange) with the π-π stacking distance of 3.56 Å (**Figure S8b**). In addition, these paired molecules displayed much shorter π-π interactions between BTD faces in an off-center parallel stacking manner with a distance of 3.40 Å without orthogonally oriented molecules. The electron deficient BTD resulted in a shorter π-π stacking distance than that of the paired molecules in a face-centered stacking. The torsional angles of **BTD-Cz** (2.82° and 5.21°) were revealed larger than that of **B-Cz** due to the more sterically crowded fjord regions.

On the other hand, indolo[3,2-*b*]carbazole-based fused-ring molecules did not show a set of paired stacking due to the two sets of α-branched alkyl side-chains on $C_{2h}$ backbones. **B-ICz** displayed weak π-π interactions in a similar manner as **B-Cz** with a distance of 3.40 Å (**Figure S8c**). In addition, this off-centered stacking layer was orthogonally sandwiched between single molecules. It was also found that the structural coplanarization of **B-ICz** in the off-centered stacking layer with a smaller torsional angle of 1.02° compared to the single molecules' torsional angle of 2.59°. In the example of **BTD-ICz**, it demonstrated alternating crossed off-centered stacking layers with the π-π stacking distance of 3.45 Å (**Figure S8d**). The crossed stacking layers were caused by weak intermolecular S···N interactions of BTD. The distance between sulfur and nitrogen was measured to be 3.53 Å, which is slightly longer than the sum of the van der Waals radii of sulfur and nitrogen atoms (3.35 Å). **BTD-ICz** also showed a larger torsional angle (3.66°) originating from the fjord regions. Interestingly, the crystal structure of **Th-ICz** did not display significant π-π interactions (**Figure S8e**). It seems that the repulsive interactions originating from electron rich thiophene hindered off-centered and edge-to-face packing modes. However, **Th-ICz** clearly exhibited intermolecular S···S interactions of thiophene on both sides, which was the main driving force of the crystal growth. The distance between sulfur and sulfur was measured to be 3.52 Å, which is slightly shorter than the sum of the van der Waals radii of sulfur (3.60 Å).

## 5. Optical Properties

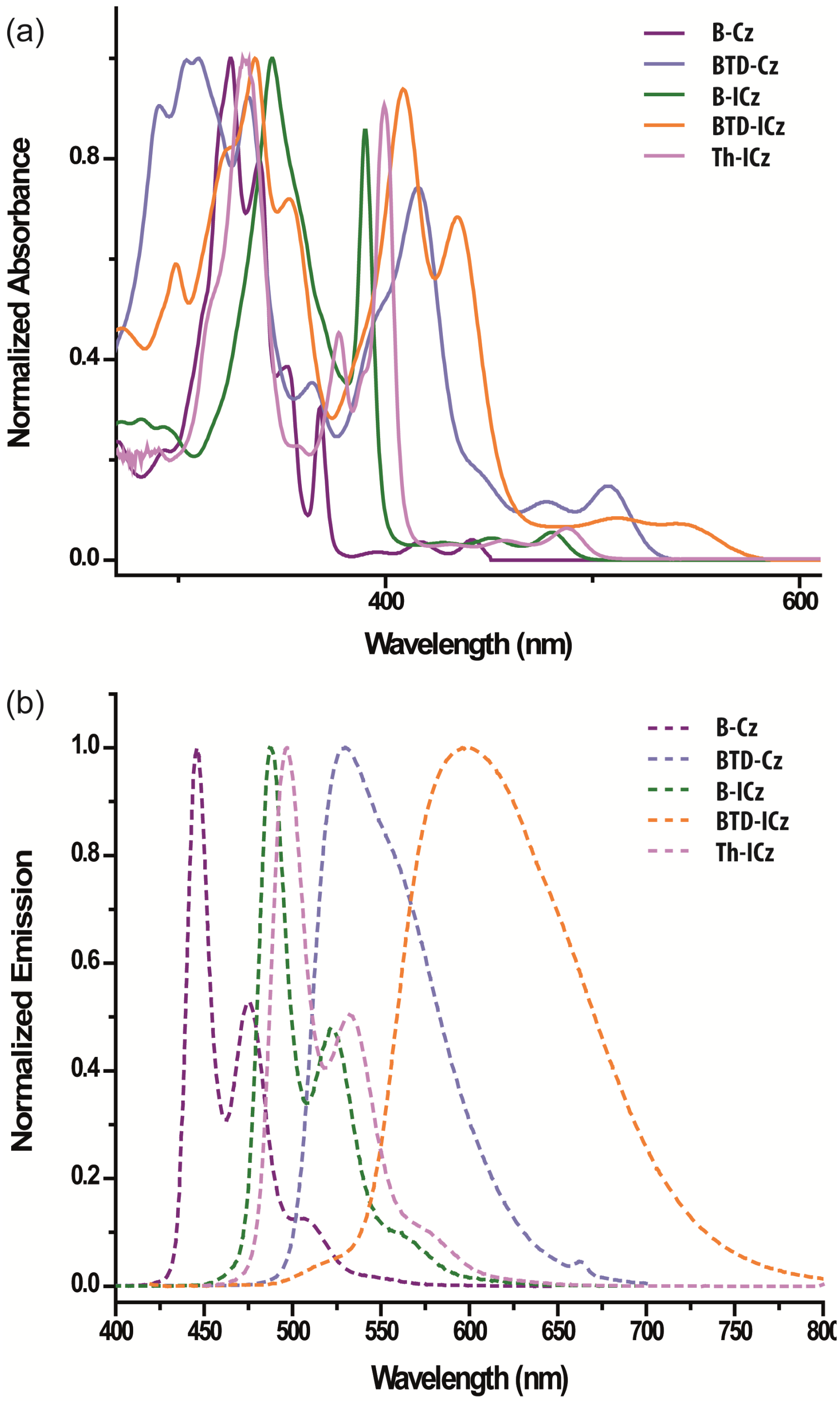

**Figure S9**. (a) UV-vis absorption and (b) fluorescence emission of **B-Cz**, **BTD-Cz**, **B-ICz**, **BTD-ICz**, and **Th-ICz** in $CHCl_3$.

## 6. Lippert-Mataga Solvatochromism Plot

Positive solvatochromism of **BTD-Cz** and **BTD-ICz** was demonstrated by a Lippert-Mataga plot using the Lippert-Mataga equation (1).[4]

$$\bar{\nu}_A - \bar{\nu}_E = \frac{2(\mu_G - \mu_E)^2}{hca^3}\Delta f + c \tag{1}$$

Herein, $\nu_A$ and $\nu_E$ are the absorption maximum and emission maximum in wavenumbers, $\mu_g$ and $\mu_E$ are, respectively, the ground and excited state dipole moments, $h$ is Planck's constant, $c$ is the speed of light in vacuum, $a$ is the Onsager cavity radius, and $\Delta f$ is the orientation polarizability. Stokes shift is generally described by the difference between absorption maximum and emission maximum. However, since **BTD-Cz** and **BTD-ICz** exhibit optically weak HOMO-LUMO transitions in the absorption spectrum, the Stokes shifts of **BTD-Cz** and **BTD-ICz** represent the difference between the weak HOMO-LUMO absorption and the emission maximum, and the difference was plotted as a function of $\Delta f$, which is defined as the equation (2).[4]

$$\Delta f = \left(\frac{\varepsilon - 1}{2\varepsilon + 1}\right) - \left(\frac{n^2 - 1}{2n^2 + 1}\right) \tag{2}$$

where, $\varepsilon$ is dielectric constant, and $n$ is refractive index of a solvent.

**Table S1**. Summary of dielectric constants ($\varepsilon$),[5] refractive indices ($n$),[5] orientation polarizabilities ($\Delta f$), absorptions, emissions, and the difference between the absorptions and emissions of **BTD-Cz** in various solvents.

| | $\varepsilon$ | $n$ | $\Delta f$ | $\lambda_{abs}$ (nm) | $\lambda_{em}$ (nm) | $\Delta \nu$ (cm$^{-1}$) |
|---|---|---|---|---|---|---|
| **Toluene** | 2.38 | 1.4969 | 0.013 | 504 | 517 | 499 |
| **Chlorobenzene** | 5.62 | 1.5248 | 0.143 | 507 | 525 | 676 |
| **Chloroform** | 4.81 | 1.4459 | 0.148 | 508 | 528 | 746 |
| **1,2-Dichlorobenzene** | 9.93 | 1.5514 | 0.186 | 509 | 530 | 778 |
| **Tetrahydrofuran** | 7.58 | 1.4072 | 0.210 | 503 | 524 | 797 |
| **Dichloromethane** | 8.93 | 1.4242 | 0.217 | 505 | 528 | 863 |
| **1,2-Dichloroethane** | 10.37 | 1.4448 | 0.221 | 506 | 532 | 966 |

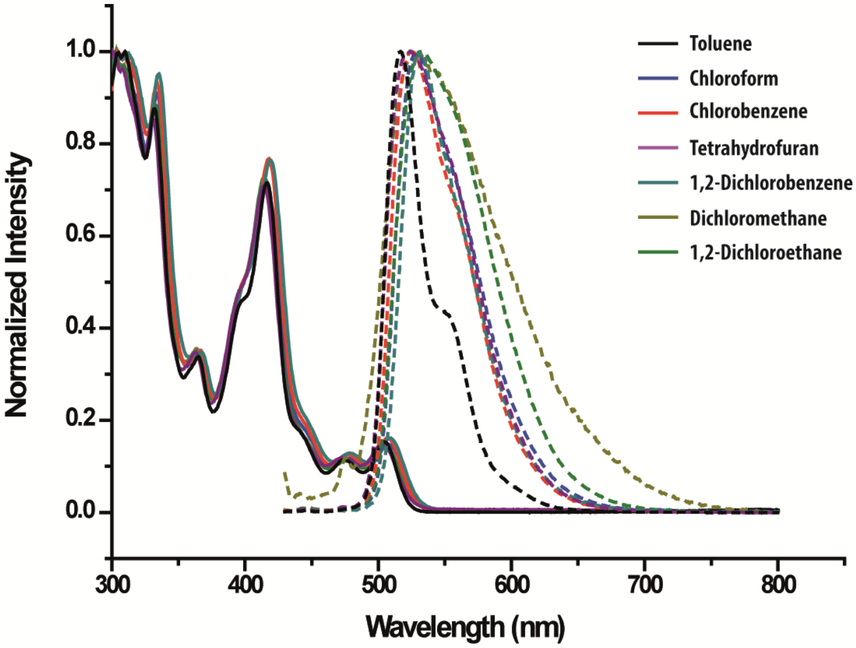

**Figure S10**. Absorption and fluorescence emission spectra of **BTD-Cz** in different solvents.

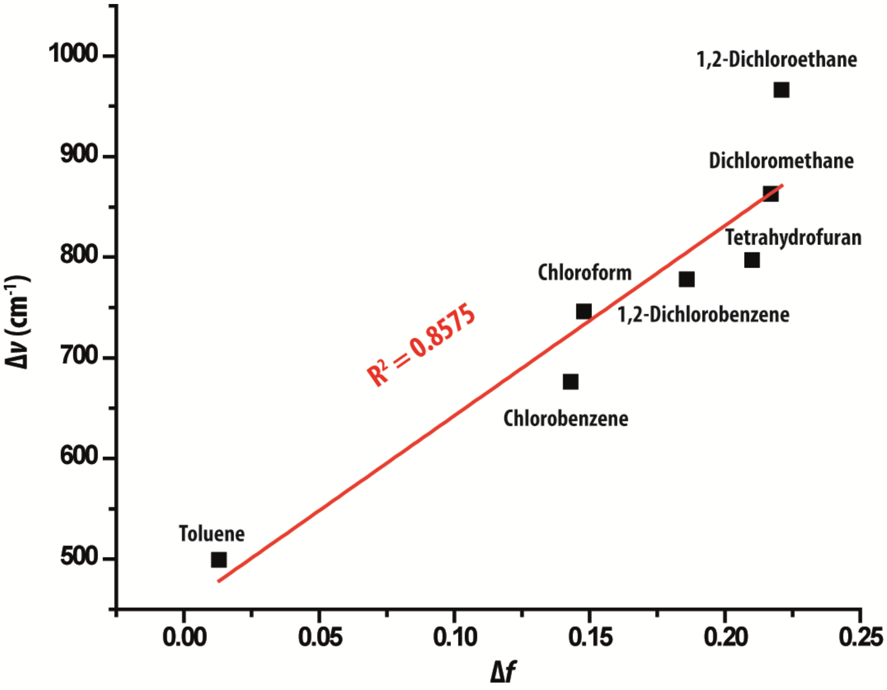

**Figure S11**. Lippert-Mataga plot of **BTD-Cz**. The red line represents the linear fit ($R^2 = 0.8575$).

**Table S2**. Summary of dielectric constants (*ε*),[5] refractive indices (*n*),[5] orientation polarizabilities (Δ*f*), absorptions, emissions, and the difference between the absorptions and emissions of **BTD-ICz** in various solvents.

| | *ε* | *n* | Δ*f* | $\lambda_{abs}$ (nm) | $\lambda_{em}$ (nm) | Δ*v* ($cm^{-1}$) |
|---|---|---|---|---|---|---|
| **Toluene** | 2.38 | 1.4969 | 0.013 | 539 | 561 | 728 |
| **Chlorobenzene** | 5.62 | 1.5248 | 0.143 | 540 | 583 | 1366 |
| **Chloroform** | 4.81 | 1.4459 | 0.148 | 540 | 598 | 1796 |
| **1,2-Dichlorobenzene** | 9.93 | 1.5514 | 0.186 | 541 | 600 | 1818 |
| **Tetrahydrofuran** | 7.58 | 1.4072 | 0.210 | 534 | 592 | 1835 |
| **Dichloromethane** | 8.93 | 1.4242 | 0.217 | 535 | 611 | 2325 |
| **1,2-Dichloroethane** | 10.37 | 1.4448 | 0.221 | 536 | 611 | 2290 |

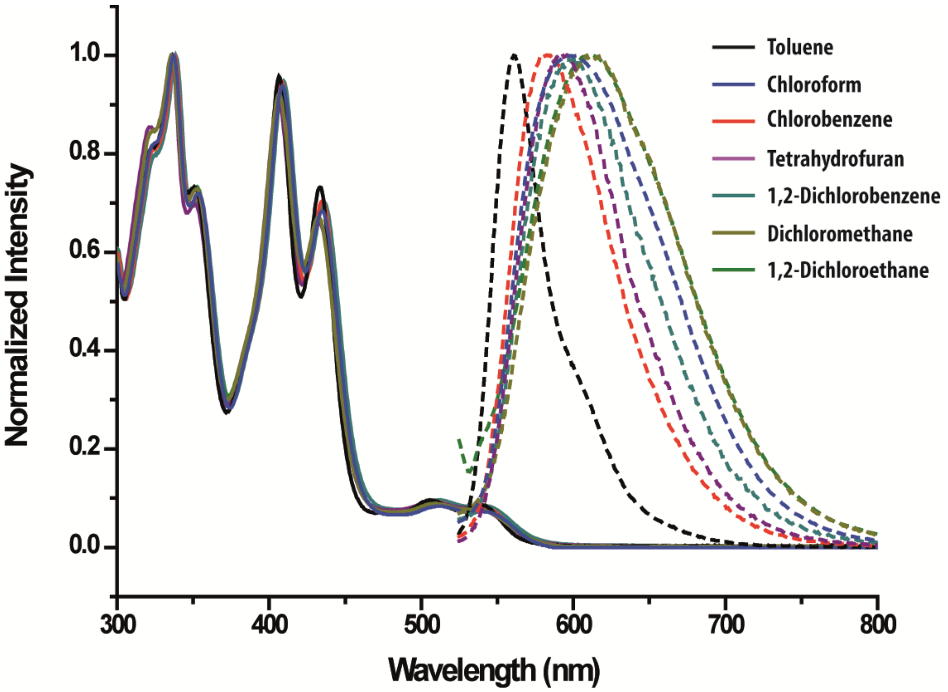

**Figure S12**. UV-vis absorption and fluorescence emission spectra of **BTD-ICz** in different solvents.

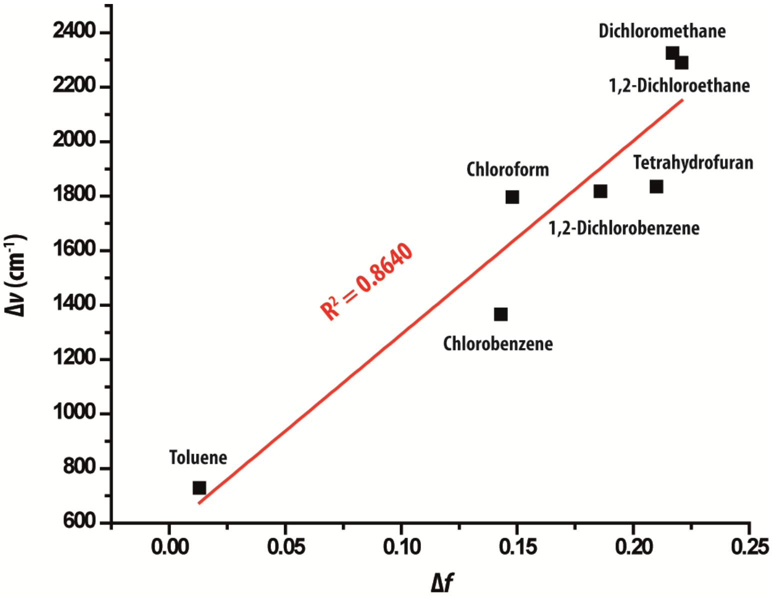

**Figure S13**. Lippert-Mataga plot of **BTD-ICz**. The red line represents the linear fit ($R^2$ = 0.8640).

## 7. Cyclic Voltammetry (CV)

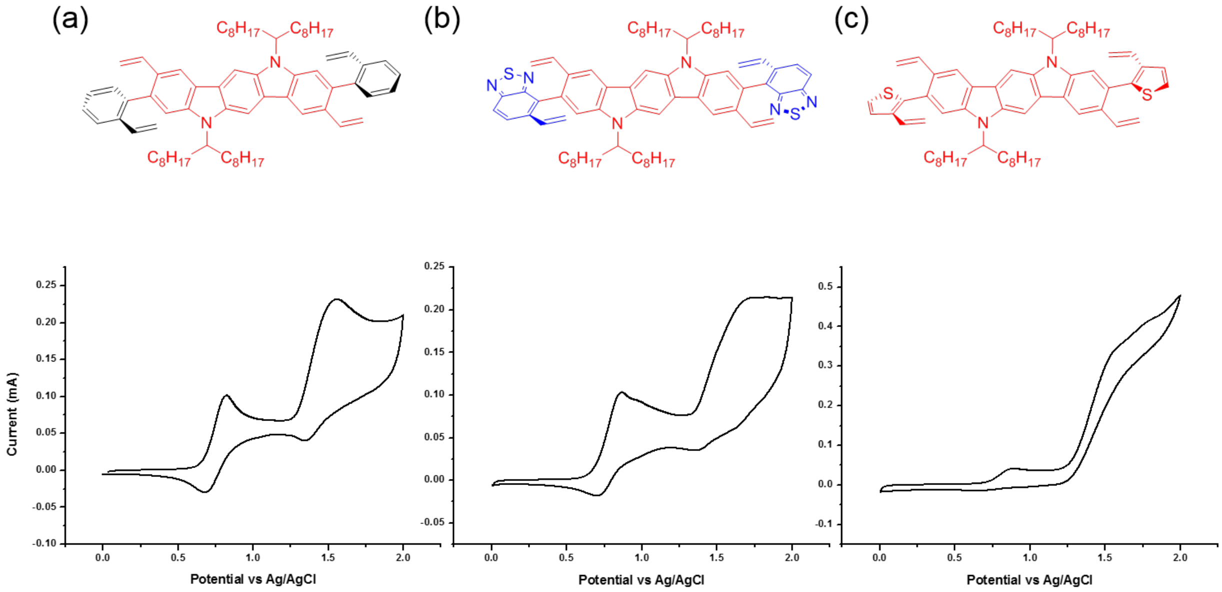

**Figure S14**. Cyclic voltammograms of (a) **2**, (b) **3**, and (c) **4** in DCM (0.1 M [*n*-$Bu_4N$]$PF_6$) at scan rate of 20 mV/s.

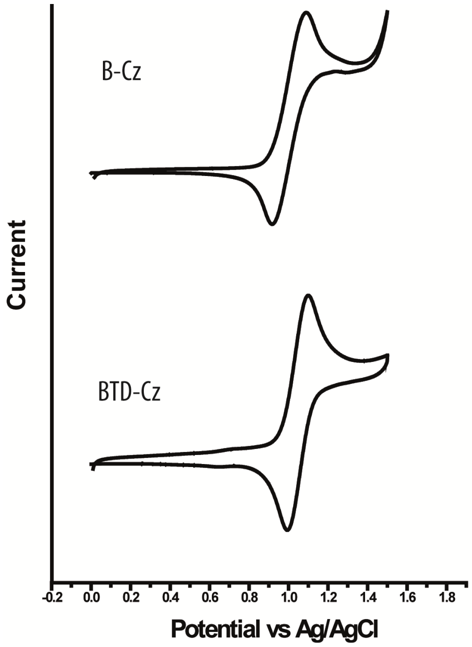

**Figure S15**. Cyclic voltammograms of (a) **B-Cz** and **BTD-Cz** in DCM (0.1 M [*n*-$Bu_4N$]$PF_6$) at scan rate of 20 mV/s.

**Table S3**. HOMO and LUMO levels of **B-Cz**, **BTD-Cz**, **B-ICz**, **BTD-ICz**, and **Th-ICz**.

| Compound | HOMO (eV) | LUMO (eV)[a] | HOMO$^{cal}$ (eV)[b] | LUMO$^{cal}$ (eV)[b] | $E_g^{opt}$ (eV)[c] |
|---|---|---|---|---|---|
| **B-Cz** | -5.32 | -2.58 | -5.23 | -1.72 | 2.74 |
| **BTD-Cz** | -5.36 | -3.02 | -5.39 | -2.63 | 2.34 |
| **B-ICz** | -5.01 | -2.50 | -4.95 | -1.78 | 2.51 |
| **BTD-ICz** | -5.02 | -2.87 | -5.05 | -2.56 | 2.15 |
| **Th-ICz** | -5.00 | -2.54 | -4.93 | -1.86 | 2.46 |

[a] LUMO was calculated by HOMO + $E_g^{opt}$. [b] HOMO and LUMO were calculated at B3LYP/6-311G(d,p). [c] Optical band gap was obtained by absorption edge from the UV-vis spectra (**Figure S9a**).

## 8. Powder X-Ray Diffraction (PXRD)

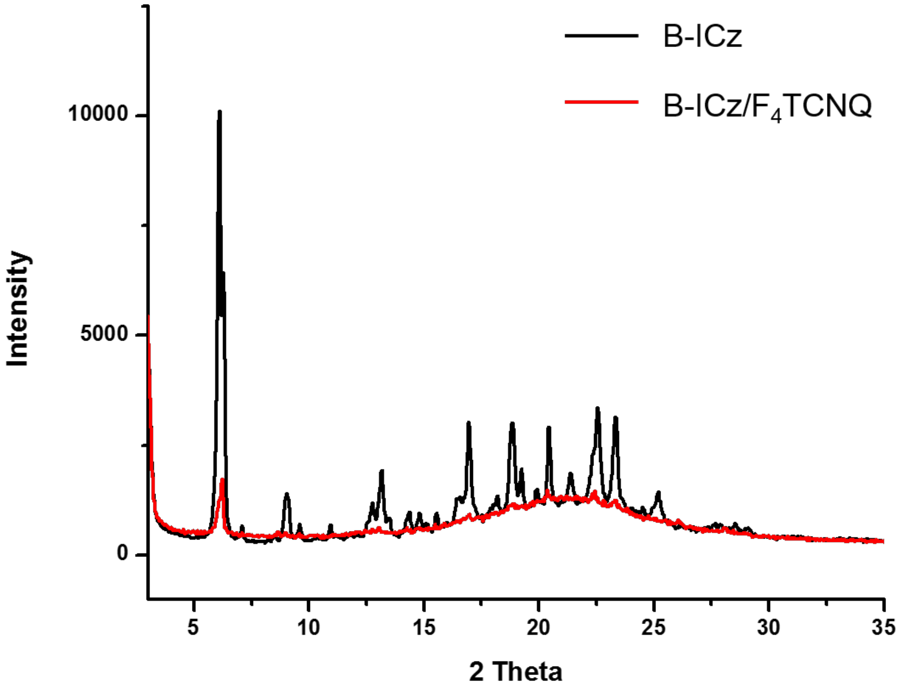

**Figure S16**. Powder X-ray diffraction of **B-ICz** (black) and **B-ICz**/F4TCNQ (red).

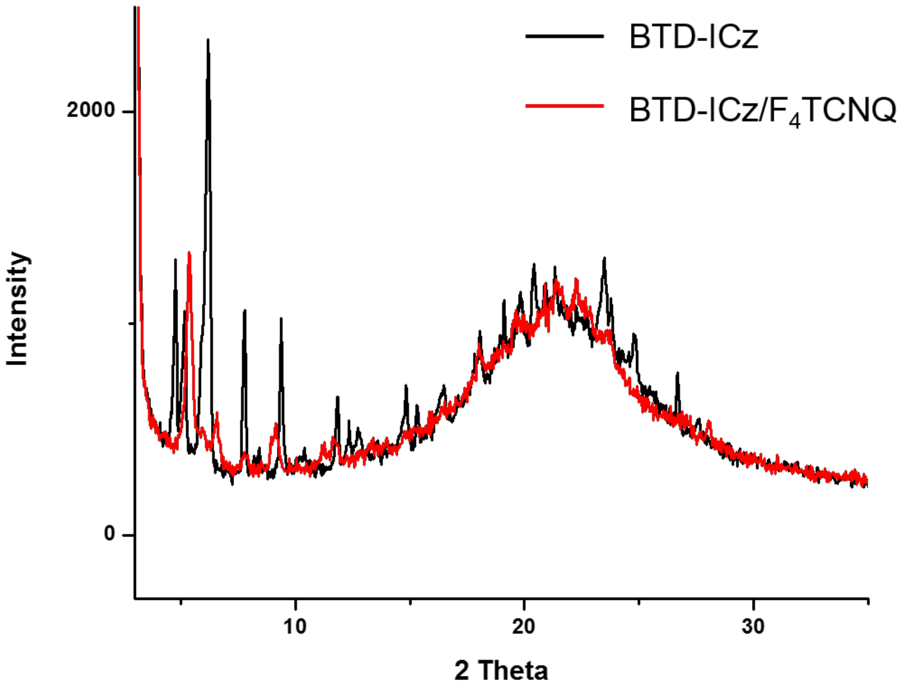

Figure S17. Powder X-ray diffraction of **BTD-ICz** (black) and **BTD-ICz**/F4TCNQ (red).

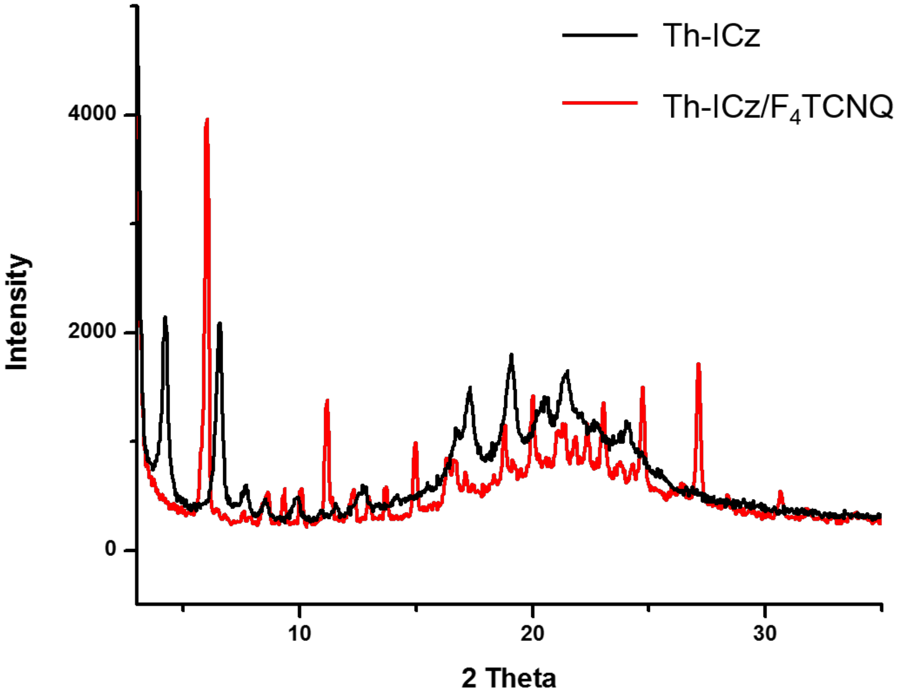

Figure S18. Powder X-ray diffraction of **Th-ICz** (black) and **Th-ICz**/F4TCNQ (red).

## 9. UV-vis-NIR Spectroscopy

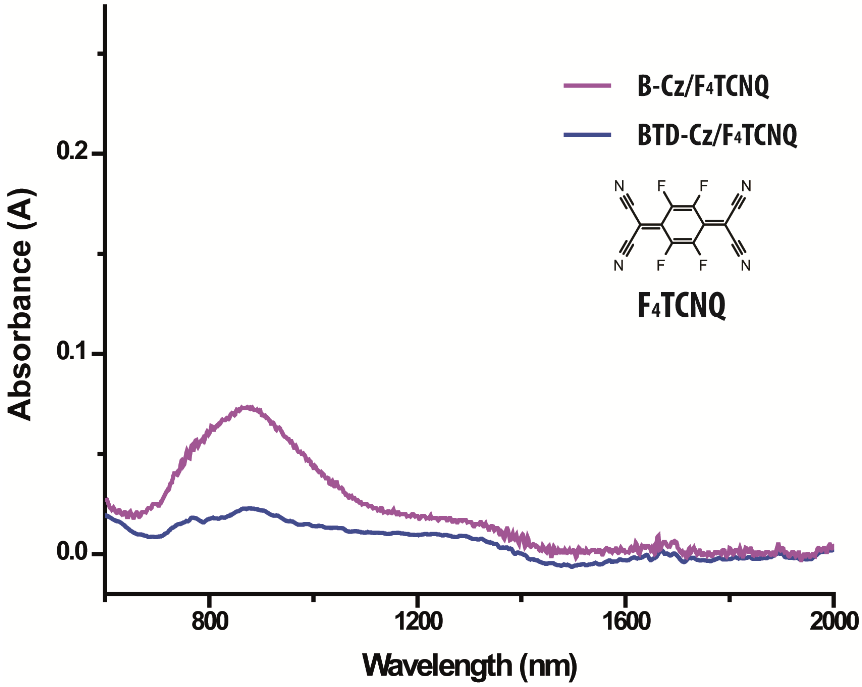

**Figure S19**. UV-vis-NIR spectrum of **B-Cz**/$F_4$TCNQ and **BTD-Cz**/$F_4$TCNQ in *o*-DCB (conc.: $2.5 \times 10^{-3}$ M, molar ratio = 1 : 1).

## 10. Electron Paramagnetic Resonance (EPR) Spectroscopy

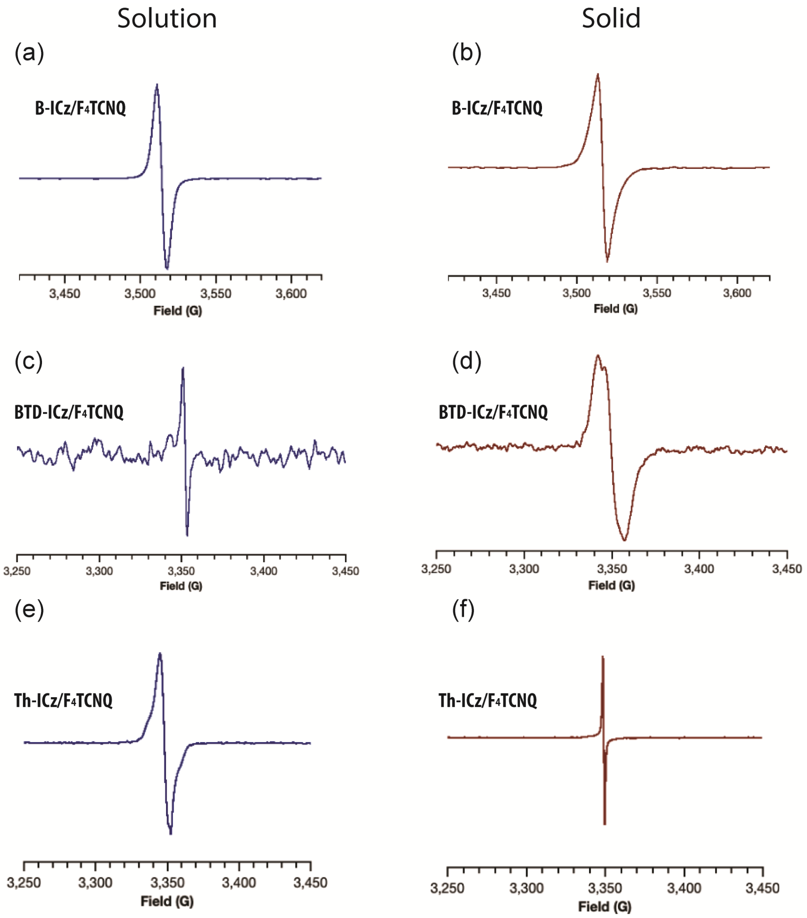

**Figure S20**. (a), (c), (e) Solution state and (b), (d), (f) the solid state of EPR spectra of **B-ICz**/$F_4$TCNQ, **BTD-ICz**/$F_4$TCNQ, and **Th-ICz**/$F_4$TCNQ, respectively.

**Table S4**. Summary of EPR spectra

| **Compound** | **State** | **P (GHz)** | **Field (mT)** | **G factor** | **Spin (1/mL)** |
|---|---|---|---|---|---|
| **B-ICz/**<br>$F_4$TCNQ | Solution | 9.85112 | 351.426 | 2.0028 | 2.458e17 |
|  | Solid | 9.85720 | 351.587 | 2.0031 | -[b] |
| **BTD-ICz/**<br>$F_4$TCNQ | Solution | 9.38330 | 335.252 | 1.9998[a] | -[a] |
|  | Solid | 9.38990 | 334.972 | 2.0028 | -[b] |
| **Th-ICz/**<br>$F_4$TCNQ | Solution | 9.38427 | 334.740 | 2.0030 | 9.499e16 |
|  | Solid | 9.38802 | 334.897 | 2.0029 | -[b] |

[a] S/N ratio was too low to be accurately measured. [b] Spin concentration was too low to integrate.

## 11. $^1$H and $^{13}$C NMR Spectra

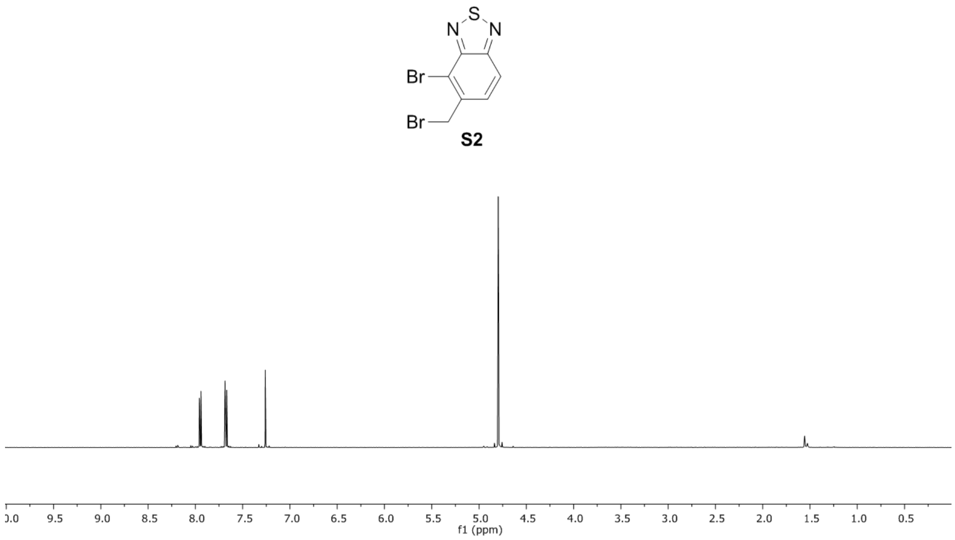

**Figure S21**. $^1$H NMR of **S2** (500 MHz, $CDCl_3$, RT).

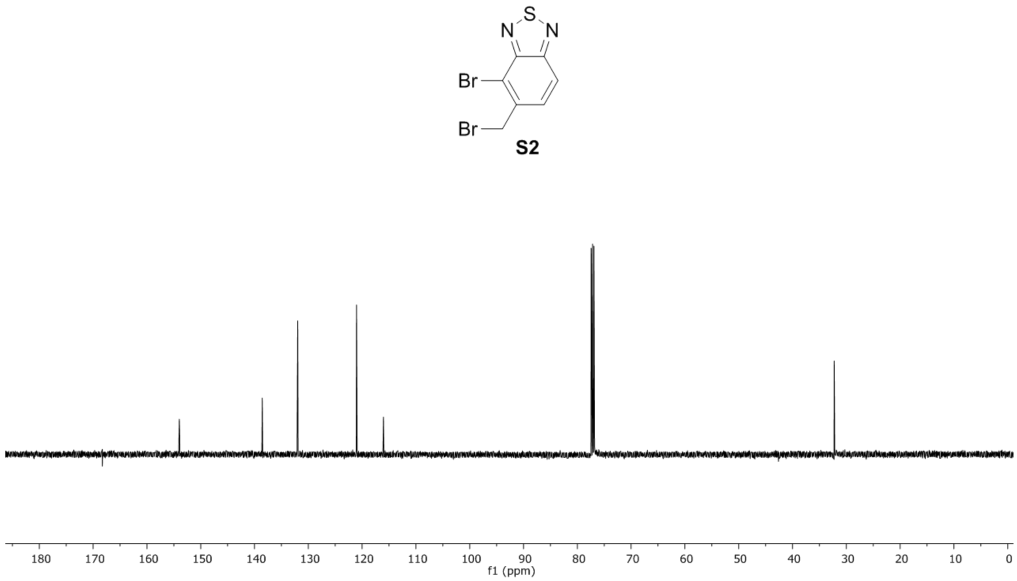

**Figure S22**. $^{13}$C NMR of **S2** (500 MHz, $CDCl_3$, RT).

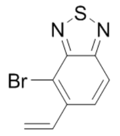

**S3**

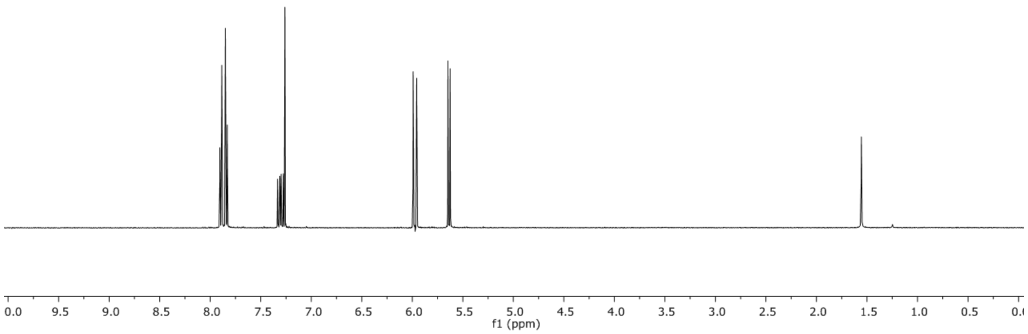

**Figure S23**. $^1$H NMR of **S3** (500 MHz, CDCl$_3$, RT).

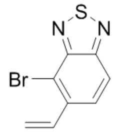

**S3**

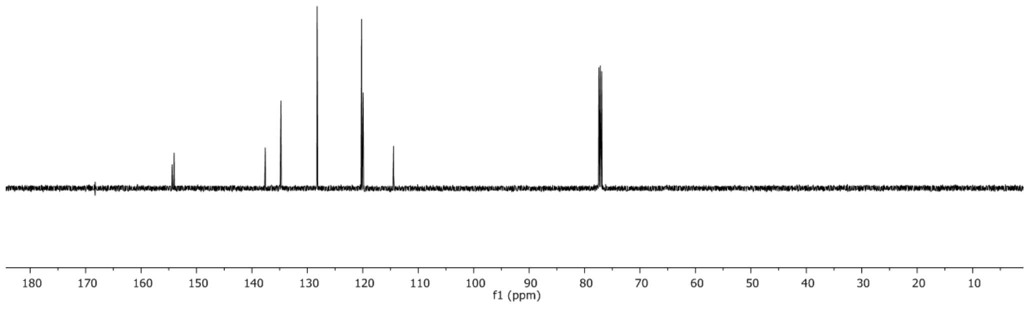

**Figure S24**. $^{13}$C NMR of **S3** (500 MHz, CDCl$_3$, RT).

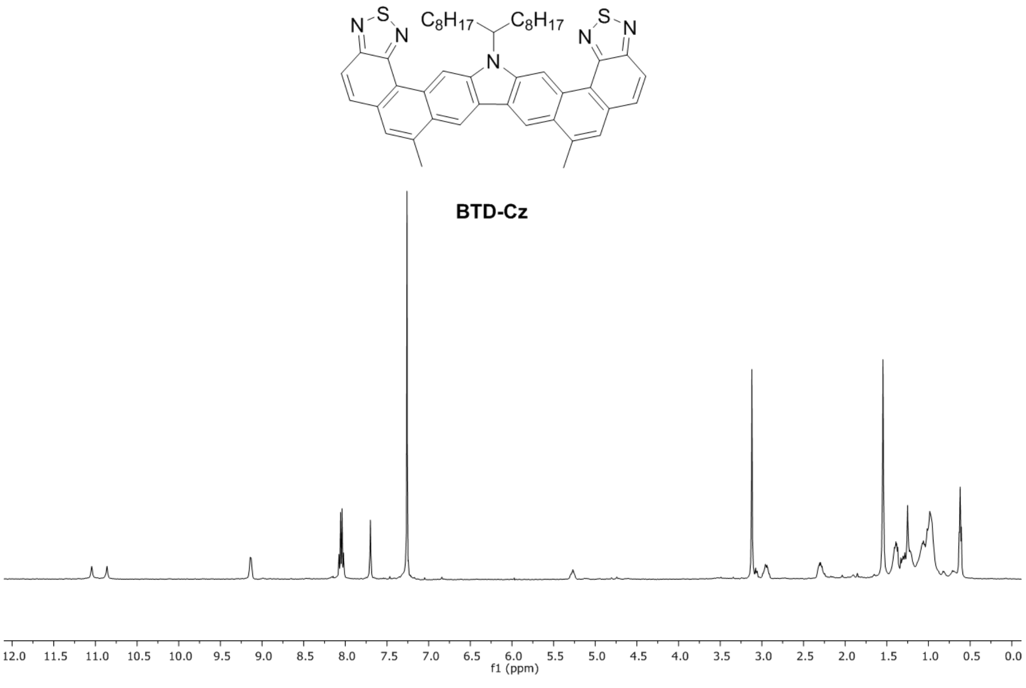

**Figure S25**. $^{1}$H NMR of **BTD-Cz** (500 MHz, $CDCl_3$, RT).

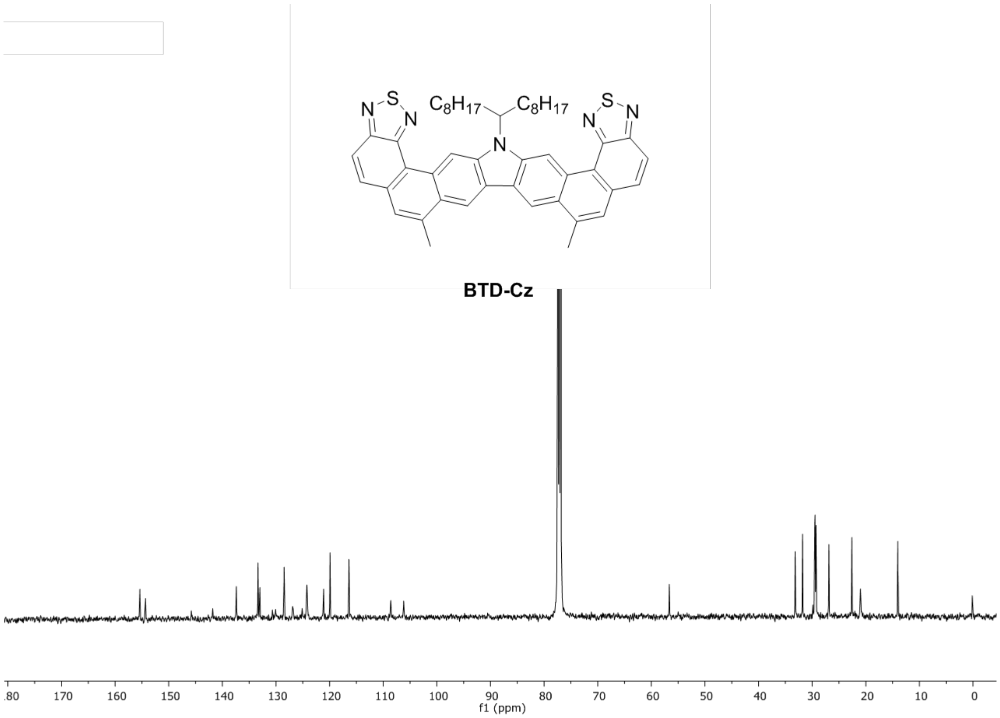

**Figure S26**. $^{13}$C NMR of **BTD-Cz** (500 MHz, $CDCl_3$, RT).

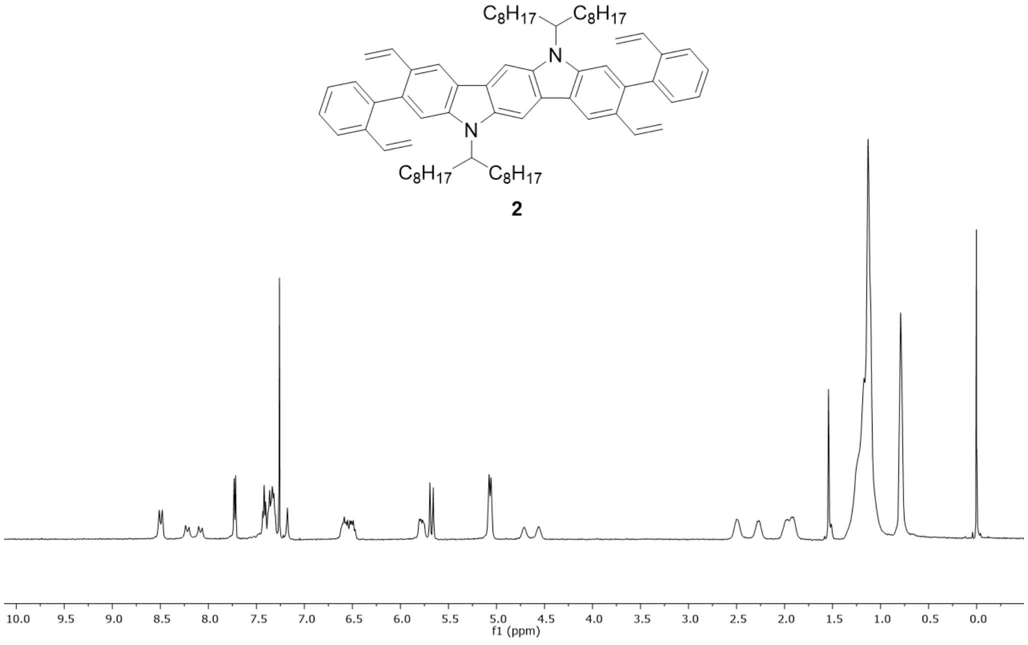

**Figure S27**. $^{1}$H NMR of **2** (500 MHz, $CDCl_3$, RT).

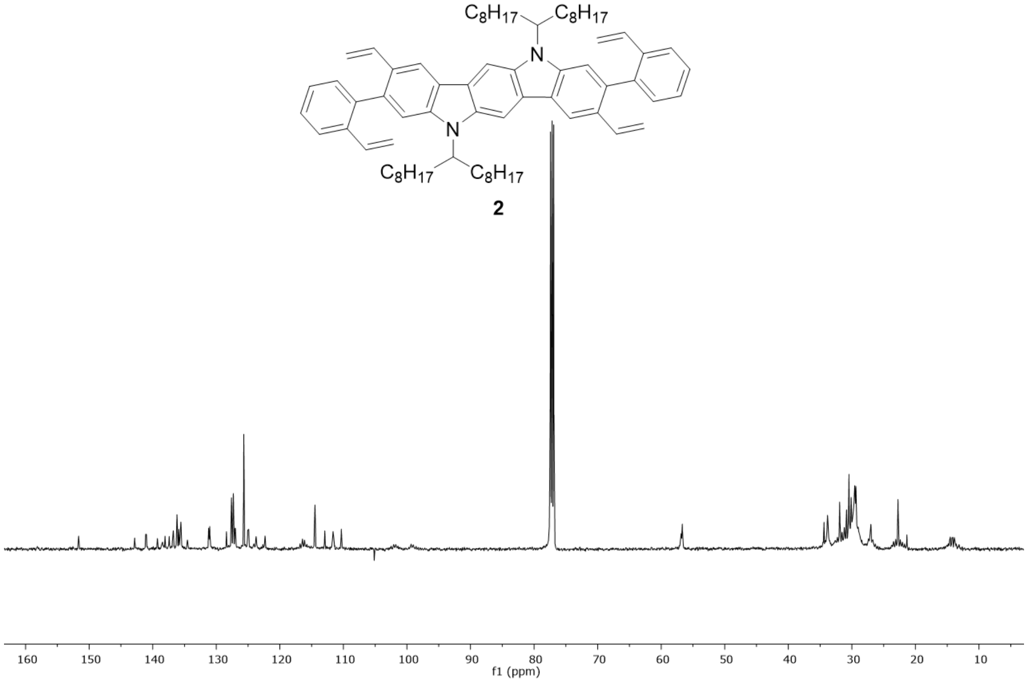

**Figure S28**. $^{13}$C NMR of **2** (500 MHz, $CDCl_3$, RT).

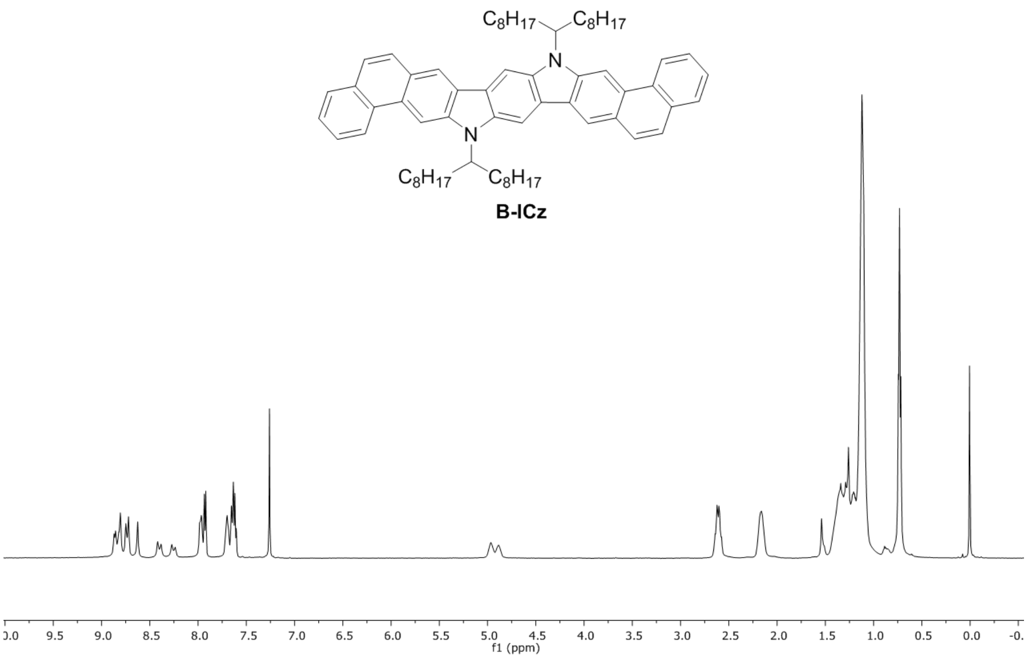

**Figure S29**. $^1$H NMR of **B-ICz** (500 MHz, $CDCl_3$, RT).

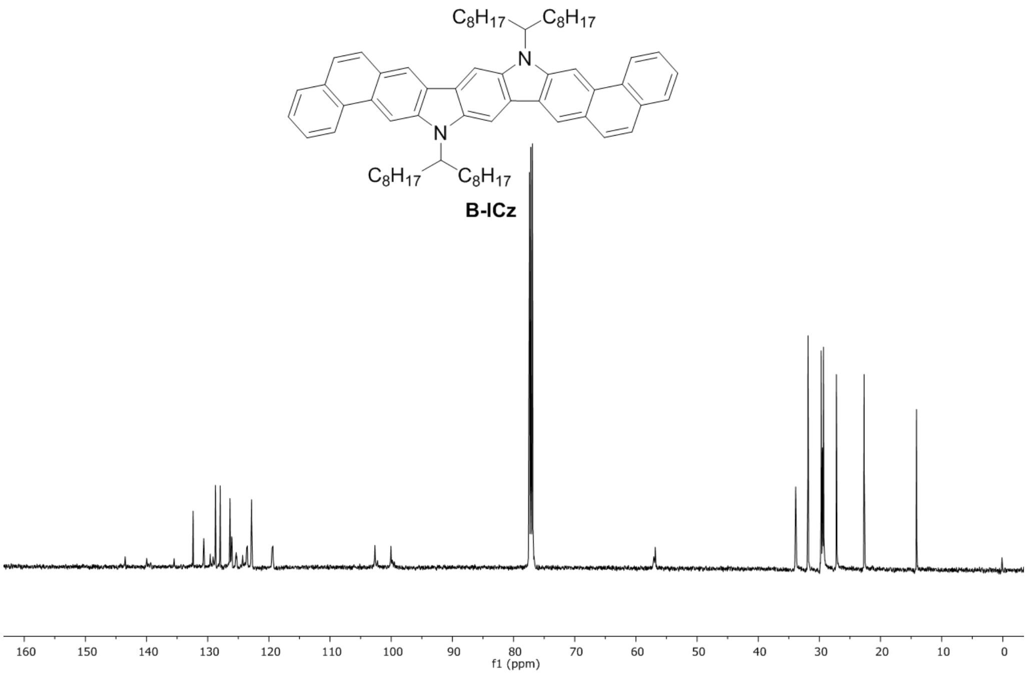

**Figure S30**. $^{13}$C NMR of **B-ICz** (500 MHz, $CDCl_3$, RT).

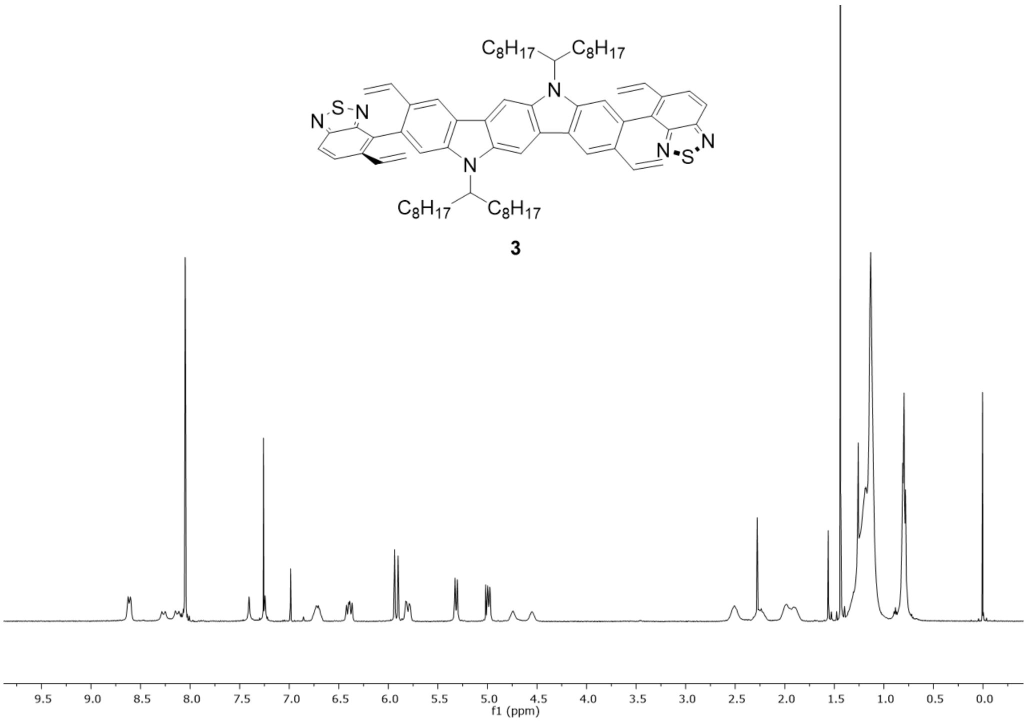

**Figure S31**. $^{1}$H NMR of **3** (500 MHz, CDCl$_3$, RT).

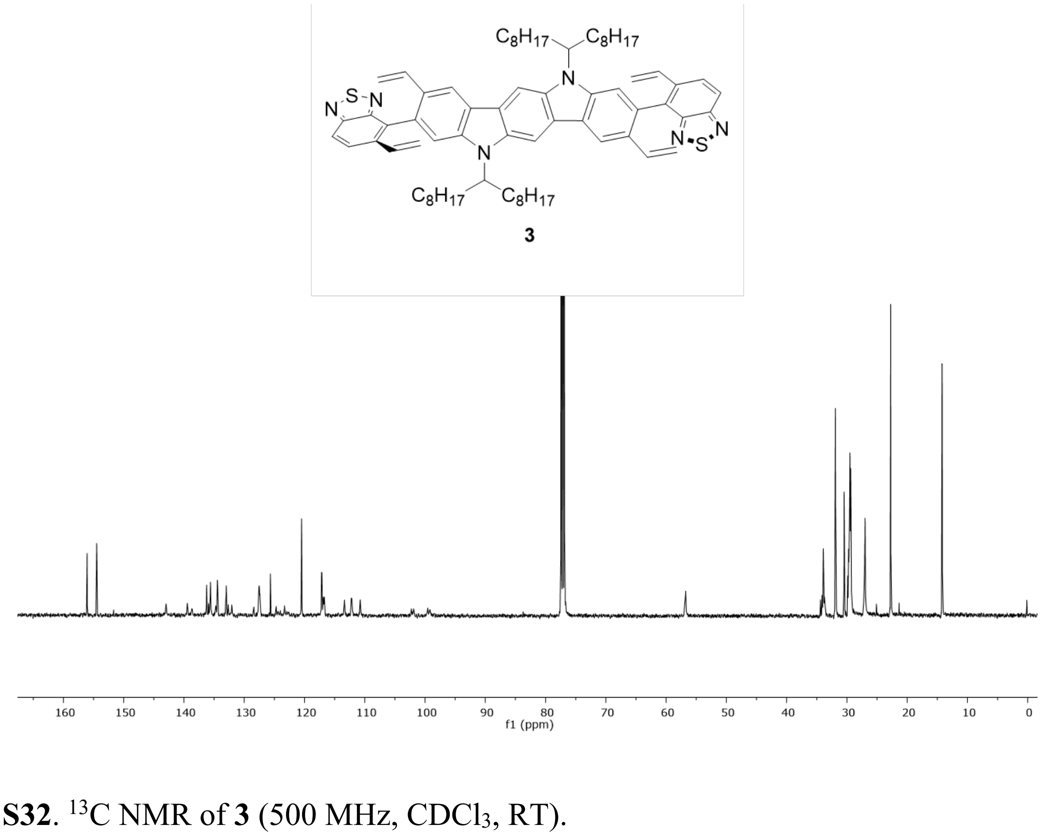

**Figure S32**. $^{13}$C NMR of **3** (500 MHz, CDCl$_3$, RT).

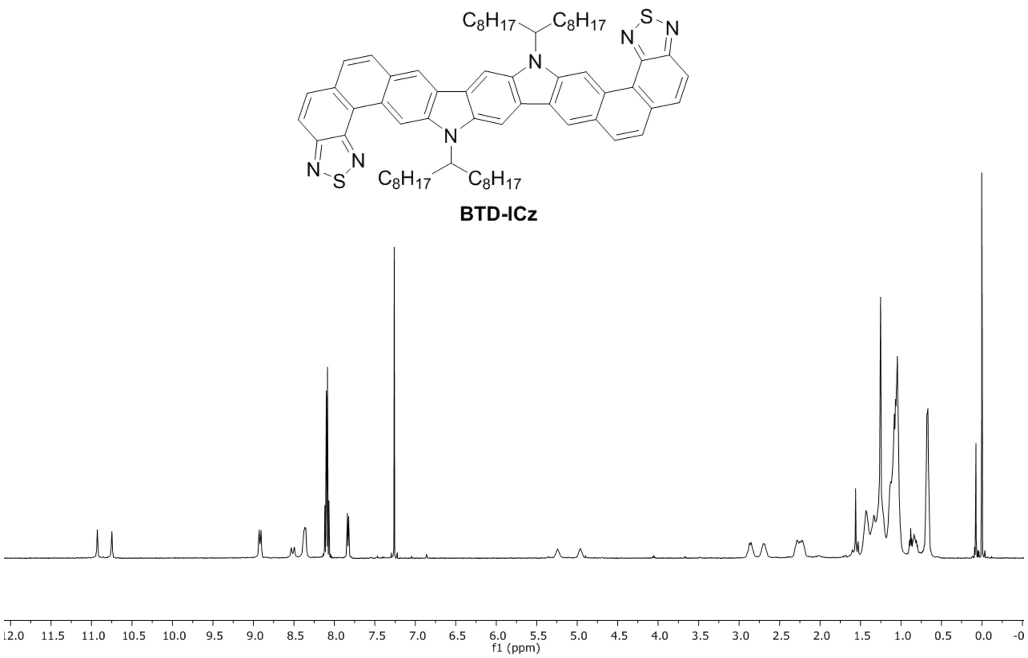

**Figure S33**. $^{1}$H NMR of **BTD-ICz** (500 MHz, $CDCl_3$, RT).

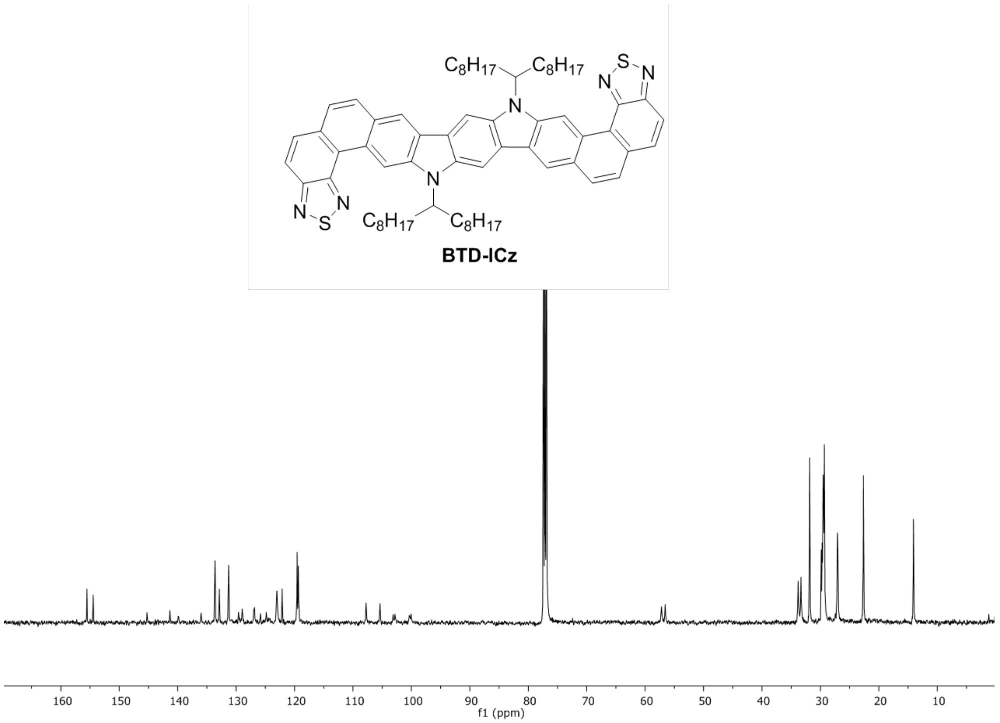

**Figure S34**. $^{13}$C NMR of **BTD-ICz** (500 MHz, $CDCl_3$, RT).

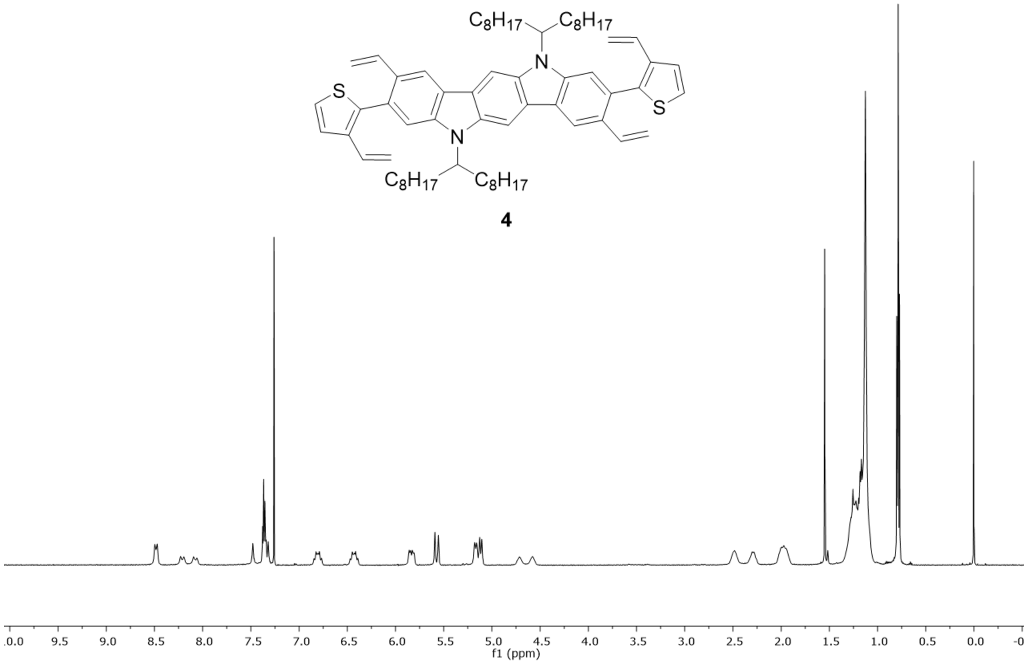

**Figure S35**. $^{1}H$ NMR of **4** (500 MHz, $CDCl_3$, RT).

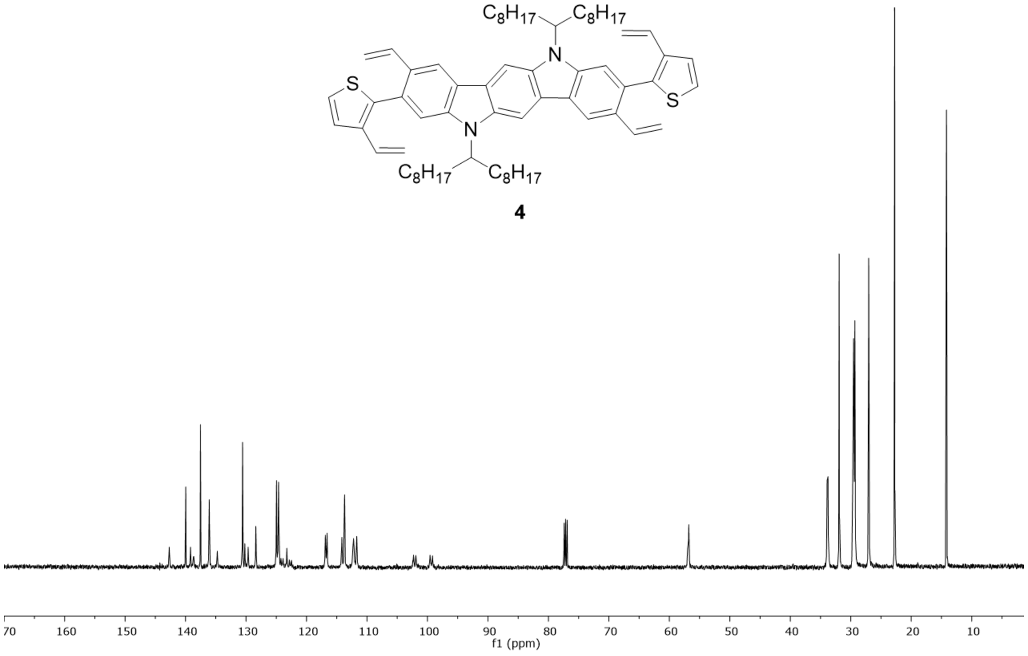

**Figure S36**. $^{13}C$ NMR of **4** (500 MHz, $CDCl_3$, RT).

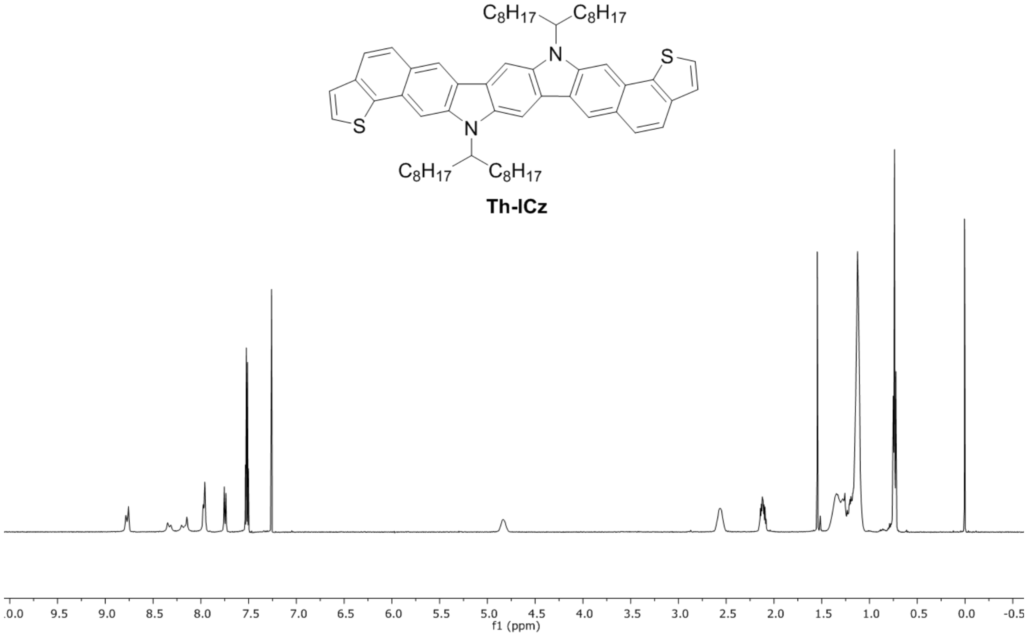

**Figure S37**. $^{1}$H NMR of **Th-ICz** (500 MHz, CDCl$_3$, RT).

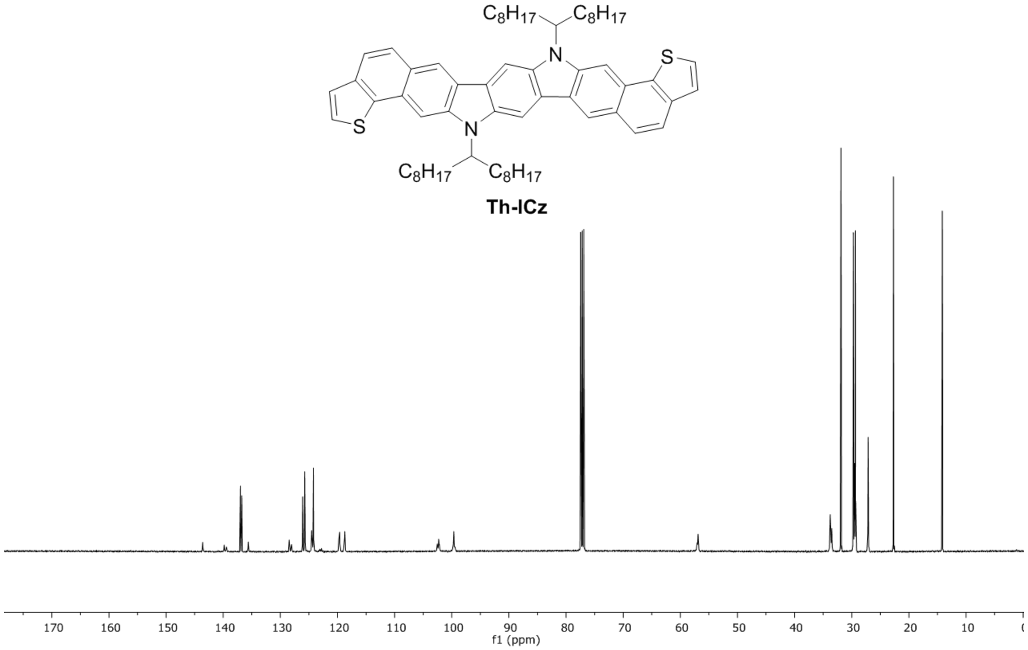

**Figure S38**. $^{13}$C NMR of **Th-ICz** (500 MHz, CDCl$_3$, RT).

## 12. Reference

1. Lee, J.; Rajeeva, B. B.; Yuan, T.; Guo, Z. -H.; Lin, Y. -H.; Al-Hashimi, M.; Zheng, Y.; Fang, L., *Chem. Sci.*, **2016**, *7*, 881-889.
2. Lee, J.; Kalin, A. J.; Wang, C.; Early, J. T.; Al-Hashimi, M.; Fang, L., *Polym. Chem.*, **2018**, *9*, 1603-1609.
3. Pilgram, K.; Zupan, M.; Skiles, R., *J. Heterocycl. Chem.*, **1970**, *7*, 629-633.
4. Pracht, P.; Bohle, F.; Grimme, S., *Phys. Chem. Chem. Phys.* **2020**, 22 (14), 7169-7192.
5. Bannwarth, C.; Ehlert, S.; Grimme, S., *J. Chem. Theory Comp.* **2019**, *15*, 1652.
6. Grimme, S.; Bannwarth, C.; Shushkov, P., *J. Chem. Theory Comp.* **2017**, *13*, 1989.
7. Philipp, P.; Eike, C.; Sebastian, E.; Stefan, G., A Robust Non-Self-Consistent Tight-Binding Quantum Chemistry Method for large Molecules. **2019**.
8. Neese, F., The ORCA program system. *WIREs Comput. Mol. Sci.* **2012**, *2*, 73.
9. Neese, F., *WIREs Comput. Mol. Sci.* **2018**, *8*, e1327.
10. Khaliullin, R. Z.; Cobar, E. A.; Lochan, R. C.; Bell, A. T.; Head-Gordon, M., *J. Phys. Chem. A* 2007, 111 (36), 8753-8765.
11. Shao, Y.; Gan, Z.; Epifanovsky, E.; Gilbert, A. T. B.; Wormit, M.; Kussmann, J.; Lange, A. W.; Behn, A.; Deng, J.; Feng, X.; Ghosh, D.; Goldey, M.; Horn, P. R.; Jacobson, L. D.; Kaliman, I.; Khaliullin, R. Z.; Kuś, T.; Landau, A.; Liu, J.; Proynov, E. I.; Rhee, Y. M.; Richard, R. M.; Rohrdanz, M. A.; Steele, R. P.; Sundstrom, E. J.; Woodcock, H. L.; Zimmerman, P. M.; Zuev, D.; Albrecht, B.; Alguire, E.; Austin, B.; Beran, G. J. O.; Bernard, Y. A.; Berquist, E.; Brandhorst, K.; Bravaya, K. B.; Brown, S. T.; Casanova, D.; Chang, C.-M.; Chen, Y.; Chien, S. H.; Closser, K. D.; Crittenden, D. L.; Diedenhofen, M.; DiStasio, R. A.; Do, H.; Dutoi, A. D.; Edgar, R. G.; Fatehi, S.; Fusti-Molnar, L.; Ghysels, A.; Golubeva-Zadorozhnaya, A.; Gomes, J.; Hanson-Heine, M. W. D.; Harbach, P. H. P.; Hauser, A. W.; Hohenstein, E. G.; Holden, Z. C.; Jagau, T.-C.; Ji, H.; Kaduk, B.; Khistyaev, K.; Kim, J.; Kim, J.; King, R. A.; Klunzinger, P.; Kosenkov, D.; Kowalczyk, T.; Krauter, C. M.; Lao, K. U.; Laurent, A. D.; Lawler, K. V.; Levchenko, S. V.; Lin, C. Y.; Liu, F.; Livshits, E.; Lochan, R. C.; Luenser, A.; Manohar, P.; Manzer, S. F.; Mao, S.-P.; Mardirossian, N.; Marenich, A. V.; Maurer, S. A.; Mayhall, N. J.; Neuscamman, E.; Oana, C. M.; Olivares-Amaya, R.; O'Neill, D. P.; Parkhill, J. A.; Perrine, T. M.; Peverati, R.; Prociuk, A.; Rehn, D. R.; Rosta, E.; Russ, N. J.; Sharada, S. M.; Sharma, S.; Small, D. W.; Sodt, A.; Stein, T.; Stück, D.; Su, Y.-C.; Thom, A. J. W.; Tsuchimochi, T.; Vanovschi, V.; Vogt, L.; Vydrov, O.; Wang, T.; Watson, M. A.; Wenzel, J.; White, A.;

Williams, C. F.; Yang, J.; Yeganeh, S.; Yost, S. R.; You, Z.-Q.; Zhang, I. Y.; Zhang, X.; Zhao, Y.; Brooks, B. R.; Chan, G. K. L.; Chipman, D. M.; Cramer, C. J.; Goddard, W. A.; Gordon, M. S.; Hehre, W. J.; Klamt, A.; Schaefer, H. F.; Schmidt, M. W.; Sherrill, C. D.; Truhlar, D. G.; Warshel, A.; Xu, X.; Aspuru-Guzik, A.; Baer, R.; Bell, A. T.; Besley, N. A.; Chai, J.-D.; Dreuw, A.; Dunietz, B. D.; Furlani, T. R.; Gwaltney, S. R.; Hsu, C.-P.; Jung, Y.; Kong, J.; Lambrecht, D. S.; Liang, W.; Ochsenfeld, C.; Rassolov, V. A.; Slipchenko, L. V.; Subotnik, J. E.; Van Voorhis, T.; Herbert, J. M.; Krylov, A. I.; Gill, P. M. W.; Head-Gordon, M., *Mol. Phys.* **2015**, *113*, 184.

12. Chai, J.-D.; Head-Gordon, M., *Phys. Chem. Chem. Phys.* **2008**, *10*, 6615.

13. (a) Mataga, N.; Kubota, T., *Ber. Bunsenges. Phys. Chem.* **1971**, *75*, 603; (b) Mataga, N.; Kaifu, Y.; Koizumi, M., *Bull. Chem. Soc. Jpn.* **1956**, *29*, 465; (c) Lippert, E. Z., *Naturforschg.* **1955**, *10a*, 541.

14. Montalti, M.; Credi, A.; Prodi, L.; Gandolfi, M. T.; Handbook of Photochemistry, 3rd ed.;CRC Press:Boca Raton, **2006**